

Paleoceanography and Paleoclimatology

RESEARCH ARTICLE

10.1029/2020PA004165

Key Points:

- Laser-ablation inductively coupled-plasma mass spectrometer facilitates absolute sea surface temperature reconstructions using foraminifera with diagenetic coatings
- Tropical sea surface temperatures remained relatively stable at 24–31°C following the Miocene climate transition
- Development of an increased latitudinal temperature gradient began prior to the Late Miocene cooling

Supporting Information:

- Supporting Information S1
- Table S1
- Table S2
- Table S3
- Table S5
- Table S6
- Table S7
- Table S8
- Table S9
- Table S10
- Table S11

Correspondence to:

M. G. Nairn,
NairnMG@cardiff.ac.uk

Citation:

Nairn, M. G., Lear, C. H., Sosdian, S. M., Bailey, T. R., & Beavington-Penney, S. (2021). Tropical sea surface temperatures following the middle Miocene climate transition from laser-ablation ICP-MS analysis of glassy foraminifera. *Paleoceanography and Paleoclimatology*, 36, e2020PA004165. <https://doi.org/10.1029/2020PA004165>

Received 30 MAR 2020

Accepted 1 FEB 2021

© 2021. The Authors.

This is an open access article under the terms of the [Creative Commons Attribution](#) License, which permits use, distribution and reproduction in any medium, provided the original work is properly cited.

Tropical Sea Surface Temperatures Following the Middle Miocene Climate Transition From Laser-Ablation ICP-MS Analysis of Glassy Foraminifera

Michael G. Nairn¹ , Caroline H. Lear¹ , Sindia M. Sosdian¹ , Trevor R. Bailey² , and Simon Beavington-Penney^{3,4} 

¹School of Earth and Environmental Sciences, Cardiff University, Cardiff, UK, ²Department of Natural Sciences, Amgueddfa Cymru, National Museum Wales, Cardiff, UK, ³BG Group, Reading, UK, ⁴Now at Department of Earth and Environmental Sciences, The University of Manchester, Manchester, UK

Abstract The mid-to-late Miocene is proposed as a key interval in the transition of the Earth's climate state toward that of the modern-day. However, it remains a poorly understood interval in the evolution of Cenozoic climate, and the sparse proxy-based climate reconstructions are associated with large uncertainties. In particular, tropical sea surface temperature (SST) estimates largely rely on the unsaturated alkenone U_{37}^k proxy, which fails to record temperatures higher than 29°C, the TEX₈₆ proxy which has challenges around its calibration, and Mg/Ca ratios of poorly preserved foraminifera. We reconstruct robust, absolute, SSTs between 13.5 Ma and 9.5 Ma from the South West Indian Ocean (paleolatitude ~5.5°S) using laser-ablation inductively coupled-plasma mass spectrometer microanalysis of glassy planktic foraminiferal Mg/Ca. Employing this microanalytical technique, and stringent screening criteria, permits the reconstruction of paleotemperatures using foraminifera which although glassy, are contaminated by authigenic coatings. Our absolute estimates of 24–31°C suggest that SST in the tropical Indian Ocean was relatively constant between 13.5 and 9.5 Ma, similar to those reconstructed from the tropics using the U_{37}^k alkenone proxy. This finding suggests an interval of enhanced polar amplification between 10 and 7.5 Ma, immediately prior to the global late Miocene Cooling.

1. Introduction

The mid-late Miocene is an important interval in the evolution of global climate through the Cenozoic, representing a key period in the transition out of the warm, dynamic climate state of the Miocene Climatic Optimum (MCO) into a more stable unipolar icehouse world (Badger et al., 2013; Foster et al., 2012; Greenop et al., 2014; Sosdian et al., 2018). Despite being characterized by similar to modern day atmospheric CO₂ concentrations (Foster et al., 2012; Sosdian et al., 2018; Super et al., 2018), middle Miocene mean global temperatures were likely significantly warmer than the modern day (Pound et al., 2011; Rouselle et al., 2013). This has been used to suggest a decoupling of global temperature and atmospheric CO₂ forcing (LaRiviere et al., 2012; Pagani et al., 1999), a characteristic which general circulation models struggle to simulate (Knorr et al., 2011; von der Heydt & Dijkstra, 2006). It has also been suggested that the late Miocene was an additional important key step in the transition to our modern climate state, as high latitudes cooled more than low latitudes, leading to a marked steepening of latitudinal temperature gradients (Herbert et al., 2016).

The late Miocene Cooling (LMC) between ~ 7.5 and 5.5 Ma was a global phenomenon (Herbert et al., 2016) perhaps associated with decreasing atmospheric pCO₂ (Stoll et al., 2019). The increase in the equator to pole surface temperature gradients was not associated with an increase in the benthic foraminiferal oxygen isotope record, implying that it occurred in the absence of a large increase in continental ice volume (Herbert et al., 2016). Polar amplification in the LMC is consistent with estimates for other time intervals (e.g., Cramwinckel et al., 2018). However, the LMC was also preceded by a significant cooling of mid to high southern and northern latitudes, a heterogeneous cooling at high northern latitudes, and a muted, limited cooling in the tropics (Herbert et al., 2016). This heterogeneous cooling perhaps suggests an unusually high polar amplification factor for the interval immediately preceding the LMC. Potential changes in the Earth System that could impact the magnitude of polar amplification include sea ice extent, vegetation induced changes in albedo, cloud cover, or ocean-atmosphere heat transport. Constraining the magnitude and timing of the

steepening of latitudinal temperature gradients is therefore important for understanding the factors driving the late Miocene surface cooling specifically, and Earth System feedbacks more generally. Ideally, this would be achieved through a combined data-modeling approach using multiproxy temperature reconstructions spanning a range of latitudes to increase confidence in calculated changes in temperature gradients.

Despite the significance of this climate interval, the evolution of global sea surface temperatures (SST) and hence temperature gradients during the mid-late Miocene is relatively poorly constrained due to a paucity of complete well-preserved sedimentary successions (Lunt et al., 2008). The widespread carbonate dissolution, which dramatically reduced the sediment carbonate content and preservation quality in deep marine sediments, is termed the middle-late Miocene carbonate crash (Farrell et al., 1995; Jiang et al., 2007; Keller & Barron, 1987; Lübbers et al., 2019; Lyle et al., 1995). In addition to these dissolution issues, the majority of foraminifera-bearing Miocene sections are comprised of carbonate rich sediments which have undergone some degree of recrystallization. The oxygen isotopic composition of planktic foraminifera that have undergone recrystallization in seafloor sediments has been shown to be biased to colder temperatures (Pearson et al., 2001). While planktic foraminiferal Mg/Ca appears to be less affected than $\delta^{18}\text{O}$, the impact of recrystallization on reconstructed Mg/Ca sea surface temperatures remains an additional source of uncertainty (Sexton et al., 2006). As a consequence, many mid-late Miocene absolute sea surface temperature reconstructions are restricted to estimates based on the unsaturated alkenone proxy and the TEX₈₆ proxy (Herbert et al., 2016; Huang et al., 2007; LaRiviere et al., 2012; Rousselle et al., 2013; Seki et al., 2012; Zhang et al., 2014). These records show a cooling in the late Miocene which begins around 10 Ma at high northern and southern latitudes. However, significant cooling in the tropics is not apparent in the alkenone records until ~7.5 Ma, while atmospheric pCO₂ reconstructions also suggest a significant decline from this time (Sosdian et al., 2018; Stoll et al., 2019). At face value therefore, these records imply an interval of enhanced polar amplification between 10 Ma and 7.5 Ma in the absence of significant drawdown of CO₂ or increase in ice volume (Herbert et al., 2016; Sosdian et al., 2018). One significant caveat to this interpretation is that the Uk₃₇ alkenone proxy becomes saturated above 28°C (Müller et al., 1998) and the late Miocene tropical SSTs prior to 7.5 Ma are at this limit (Herbert et al., 2016). Therefore, an alternative interpretation of the data would be that the high latitudes and the tropics cooled synchronously from ~10 Ma, but the initial cooling in the tropics was not able to be recorded by the Uk₃₇ alkenone proxy. Corroboration of the absolute Uk₃₇ alkenone temperatures by an independent proxy would therefore confirm the timing of the global late Miocene Cooling and the possible interval of enhanced polar amplification between 10 and 7.5 Ma.

Here we present a new planktic foraminiferal Mg/Ca record from the Sunbird-1 industry well cored offshore Kenya by BG Group. Critically, middle to late Miocene sediments in Sunbird-1 are hemipelagic clays, which has resulted in glassy preservation of the foraminifera. However, the foraminifera are coated with metal-rich authigenic coatings, which are not removed by standard cleaning techniques. Planktic foraminifera were therefore analyzed by laser ablation inductively coupled-plasma mass spectrometer (ICP-MS) to obtain Mg/Ca from the primary foraminiferal test and hence enable estimation of absolute SSTs.

2. Materials and Methods

2.1. Site Location, Stratigraphy, and Age Control

This study utilizes 91 cuttings, spanning 273 meters at burial depths ranging from 630 to 903 m, recovered by BG Group from the Sunbird-1 well offshore Kenya (04° 18' 13.268" S, 39° 58' 29.936" E; 723.3 m water depth) (Figure 1, Table S1). Sedimentation at Sunbird-1 through the studied interval (9.5–13.5 Ma) is dominated by clays; the fraction of the sediment >63 μm averages 11.5% (Table S1), much lower than typical carbonate-rich deep-water sites. The impermeable nature and chemical composition of clay-rich sediment reduces diagenetic alteration of primary foraminiferal calcite, making them ideal targets for geochemical analysis (Pearson et al., 2001; Sexton et al., 2006). Tests displaying the desired exceptional preservation appear glassy and translucent under reflected light, and SEM imaging shows retention of the foraminiferal original microstructure (Pearson & Burgess, 2008). This style of preferential glassy preservation, as displayed in the Sunbird-1 well, is rare to absent in published records from Miocene foraminifera.

Micropaleontological and calcareous nannoplankton assemblages for Sunbird-1 were analyzed by Haydon Bailey and Liam Gallagher of Network Stratigraphic Consulting. Biostratigraphic datums, correlated with

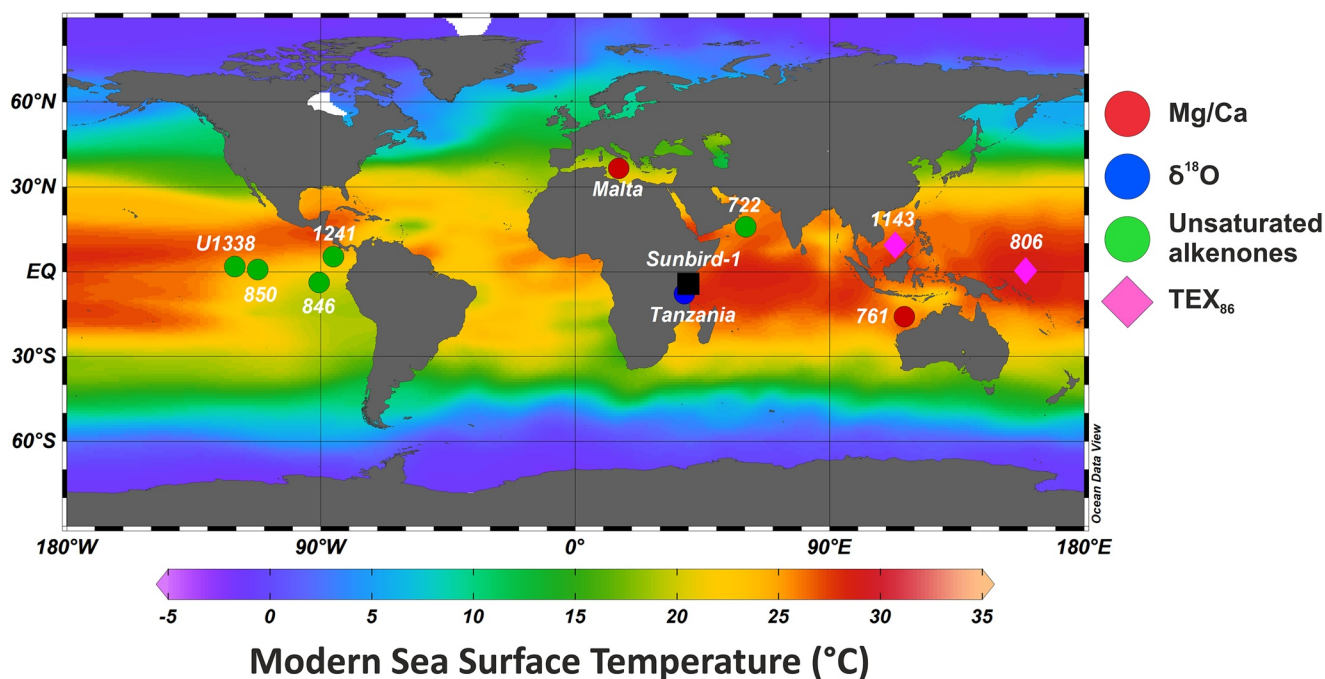


Figure 1. Location of the Sunbird-1 study site (black square). Other sites for which there are mid to late Miocene sea surface temperature reconstructions from Mg/Ca (red circles), $\delta^{18}\text{O}$ (blue circles), unsaturated alkenones (green circles) and TEX_{86} (pink diamonds) are shown. Figure produced using Ocean Data Viewer (Schlitzer, 2020) using modern-day mean annual sea surface temperature data from the World Ocean Database.

the astronomical timescale of Raffi et al. (2020), are based on the planktic foraminifera zonations of Wade et al. (2011) and calcareous nanofossil zonations of Backman et al. (2012). An age model was constructed by linear interpolation between these biostratigraphic datums (Figure S1). Sedimentation rates were ~ 3 cm/kyr immediately following the middle Miocene Climate Transition (MMCT), and subsequently increased to ~ 17 cm/kyr between 11.8 and 11.5 Ma, before decreasing to ~ 8 cm/kyr until 9.5 Ma.

2.2. Foraminiferal Stable Isotope Analysis

Up to 12 individual tests of the planktic foraminifer *Globigerinoides obliquus* showing glassy preservation were used. *G. obliquus* is an extinct, symbiont-bearing species with a tropical to subtropical paleogeographical distribution, and is interpreted as a surface mixed-layer dweller (Aze et al., 2011; Keller, 1985). The assertion that *G. obliquus* inhabits and calcifies in the surface mixed layer (Aze et al., 2011; Keller, 1985) is supported by multispecies analyses from a 10.0 Ma sediment sample from the Indian Ocean offshore Tanzania showing *G. obliquus* to have the most negative $\delta^{18}\text{O}$ (-2.5‰) of all species (Paul Pearson, personal communication, 2019). Tests were crushed between two glass plates ensuring all chambers were opened. Any visible infill was removed using a fine paintbrush under a binocular microscope. Fine clays and other detrital material on the outer surface of the test were removed by rinsing three times in 18.2 MΩ DI water, ultrasonicing for 5–10 s in analytical grade methanol, and finally rinsing a further time in 18.2 MΩ DI water. Samples were analyzed at Cardiff University on a ThermoFinnigan MAT253 with online sample preparation using an automated Kiel IV carbonate device. Results are reported relative to Vienna Pee Dee Belemnite, and long-term uncertainty based on repeat analysis of NBS-19 is $\pm 0.08\text{‰}$ ($n = 469$, 2 standard deviations) and on repeat analysis of BCT63 is $\pm 0.07\text{‰}$ ($n = 310$, 2 standard deviations). Data are available in Table S2.

2.3. Solution ICP-MS Trace Metal Analysis

Between 10 and 15 individuals of the planktic foraminifer *Dentoglobigerina altispira* from the 250–355 μm size fraction were picked and weighed on a six-decimal-place balance to determine average test weight.

Individual tests were then crushed between two glass plates ensuring all chambers were opened. Due to the low foraminiferal abundance it was not possible to analyze the same species for stable isotope and trace metal composition. Any visible infill was removed using a fine paintbrush under a binocular microscope. Fragments were cleaned to remove clays and organic matter following the standard protocol (Barker et al., 2003; E. Boyle & Keigwin, 1985). Due to the clay-rich nature of the sediment the clay removal procedure was conducted twice. To test for the possible presence of metal oxides half of the samples were reductively cleaned between the clay removal and oxidative cleaning steps. Samples were dissolved in trace metal pure 0.065 M HNO₃ and diluted with trace metal pure 0.5 M HNO₃ to a final volume of 350 μ l. Samples were analyzed at Cardiff University on a Thermo Element XR ICP-MS using standards with matched calcium concentrations to reduce matrix effects (Lear et al., 2002, 2010). Together with Mg/Ca, several other ratios (Al/Ca, Mn/Ca, and U/Ca) were analyzed to screen for potential contaminant phases. Data are available in Table S3. Long-term analytical precision for Mg/Ca throughout the study is better than 2%.

2.4. Laser Ablation-ICP-MS Analysis

Direct sampling of solid phase material via laser ablation (LA-) allows for geochemical analyses through individual foraminiferal tests at the submicron scale when coupled to an ICP-MS (Detlef et al., 2019; S. M. Eggins et al., 2004; Evans, Erez, et al., 2015; Fehrenbacher et al., 2015; Hines et al., 2017; Petersen et al., 2018; Reichart et al., 2003). A key advantage of analyzing the trace element composition of foraminifera using LA-ICP-MS over the more traditional solution-based ICP-MS is the ability to recognize the diagenetically altered portions of the tests, allowing identification of the primary calcite (Crech et al., 2010; Hasenfratz et al., 2016; Pena et al., 2005). The elemental composition of this primary calcite can provide important information about palaeotemperature (S. Eggins et al., 2003; de Nooijer et al., 2017; Pena et al., 2005) and other paleo-environmental conditions such as pH (Mayk et al., 2020; Thil et al., 2016) and oxygenation (Koho et al., 2015; Petersen et al., 2018).

Up to six specimens of *D. altispira* per sample were selected from 44 depth intervals through the Sunbird-1 core for LA-ICP-MS analysis. Foraminiferal sample preparation included the removal of fine clays and other detrital material on the outer surface of the test using DI water and methanol, but the more aggressive oxidative and reductive steps (Barker et al., 2003; E. Boyle & Keigwin, 1985), were not required for laser ablation analysis (Vetter et al., 2013). The cleaned tests were mounted onto glass slides using double sided carbon tape and were allowed to dry before being mounted into the sample cell (Evans, Bhatia, et al., 2015; Fehrenbacher et al., 2015; Hines et al., 2017).

Analyses were performed using an ArF excimer (193 nm) LA-system with dual-volume laser-ablation cell (RESOLUTION S-155, Australian Scientific Instruments) coupled to a Thermo Element XR ICP-MS. Optimized ablation parameters and analytical settings determined for analyzing foraminifera in the Cardiff University CELTIC laboratory (Table S4; Detlef et al., 2019; Nairn, 2018) were used for this study. Three cleaning pulses to remove any contaminant on the outer \sim 0.5 μ m of the test surface were included prior to analysis. We analyzed ²⁵Mg, ²⁷Al, ⁴³Ca, ⁵⁵Mn, and ⁸⁸Sr, each isotope having a constant 50 ms dwell time. Typically, intervals with elevated Mn and Al in concert with elevated Mg are interpreted as being contaminant phases (e.g., Fe-Mn oxides-hydroxides or clays), and are commonly found on the inner and outer test surface (Barker et al., 2003; de Nooijer et al., 2014; Hasenfratz et al., 2016; Koho et al., 2015; Pena et al., 2005).

Where possible, three laser spot depth profiles were collected on each of the penultimate (f-1) and previous (f-2) chambers by ablating with 100 consecutive laser pulses in one position on the test. Assuming that each laser pulse only ablates a \sim 0.1 μ m layer of calcite (S. Eggins et al., 2003), we estimate the profile to represent a transect through the test wall approximately 15 μ m long. However, in some cases older chambers were required to ensure six laser profiles per specimen were analyzed (Nairn, 2018). NIST SRM 610 glass standard was measured between every six laser profiles, and NIST SRM 612 at the beginning and end of analyses from each sample depth. The reference values for elemental concentrations in both silicate glass standards are taken from the GEOREM website (http://georem.mpch-mainz.gwdg.de/sample_query_pref.asp), updated from Jochum, Weis, et al. (2011). NIST SRM 612 was used to determine long term external reproducibility using NIST SRM 610. For Mg/Ca, NIST 612 (n = 90) had an accuracy of 12.0% and a precision of 3.7% relative to the reported value. A similar \sim 12% negative offset relative to the reported value of NIST 610-calibrated NIST 612 has been observed over a much longer period of data collection (Evans &

Müller, 2018). To supplement this assessment, we also conducted accuracy tests using the GOR-132 and KL-2 MPI-DING glasses (Jochum, Wilson, et al., 2011). For this, GOR-132 and KL2 were treated as unknowns, with both NIST 610 and NIST 612 as calibration standards. For Mg/Ca, GOR-132 ($n = 25$) had an accuracy of 1.1% and a precision of 3.2% relative to the reported value, and KL-2 ($n = 25$) had an accuracy of 0.6% and a precision of 2.6% relative to the reported value when calibrated using NIST 610. These values increased to 10.9% and 9.4% for GOR-132, and 8.2% and 5.4% for KL-2 when calibrated using NIST 612. The NIST 610-calibrated data presented here supports the determination of Evans, Erez, et al. (2015) that the Mg values for NIST 612 requires reassessment.

An important issue related to accuracy is that because a well-characterized, homogenous calcite reference material is not currently available for laser ablation use, the glass standards we used have a different matrix to the calcite foraminifera tests (Evans, Erez, et al., 2015; Evans & Müller, 2018; Fehrenbacher et al., 2015). Therefore, while we have high confidence in the accuracy of the intraand interspecimen geochemical variability described in Section 2.6, we must consider the possibility of an analytical bias in the absolute geochemical composition of foraminiferal tests determined by laser ablation ICP-MS. One way to assess the magnitude of such potential bias is to analyze foraminiferal samples by both solution and laser ablation ICP-MS. However, it is important to note that the corrosive cleaning protocol for solution analysis tends to slightly lower primary test calcite Mg/Ca, an issue that is routinely circumvented by employing the same cleaning on calibration samples for paleotemperature reconstructions (Barker et al., 2003). For the purpose of this study, it is therefore important that our LA-ICP-MS technique gives values that are consistent with our samples analyzed by solution ICP-MS. We are able to make a direct comparison of our youngest samples in this way, because these do not have significant authigenic coatings biasing the solution analyses. For these samples, our solution and laser ablation results are in excellent agreement, which gives us confidence in the LA-ICP-MS values for the older samples, where we know the solution ICP-MS results are compromised by authigenic coatings (Figure S2). Furthermore, we note that if future work indicates a consistent offset between laser ablation Mg/Ca analyses of carbonates and silicate glasses, owing to their differing matrices, our standard values reported above will allow our data to be corrected to obtain an accurate composition of the uncleaned foraminiferal calcite.

2.5. LA-ICP-MS Data Processing and Screening

Each individual laser ablation profile was carefully inspected and processed using the SILLS data reduction software package (Guillong et al., 2008) following the established protocol outlined in Longerich et al. (1996). Profiles generally followed one of two patterns: (i) a rise from background values to a transient peak, followed by a somewhat lower plateau, or (ii) a rise from background values to a general plateau (Figure 2). There are two likely explanations for the initial transient peak in some isotope profiles: ablation of authigenic coatings enriched in some trace metals, or laser ablation induced isotope fractionation (so-called “pit effects”). We favor the first explanation because we used the same operating parameters on every profile, and would therefore expect any “pit effects” to be consistent among the profiles. Furthermore, profiles containing the transient peaks were more prevalent in the older part of the record, where our solution Mn/Ca analyses demonstrate the presence of authigenic coatings. Therefore, we assume the transient peaks represent contaminated portions of the test and exclude those regions. The integration interval for the profile was selected based upon the following three criteria: (i) stable ^{43}Ca counts, indicating ablation of calcite, (ii) stable Mg/Ca signal, indicating a consistent primary calcite phase, (iii) flat Mn/Ca and Al/Ca signals, avoiding any peaks indicating intervals of contamination (Figure 2).

Individual depth profiles were corrected by first subtracting the mean background signal (determined from ~15 s of data acquired when the laser was turned off prior to ablation). The repeated analysis of the NIST 610 standard reference material was used to linearly correct for any instrumental drift. Typically, this is small, <2%, because of the good counting statistics and stable data acquisition during ablation. The ablation profiles were normalized to ^{43}Ca as the internal standard and elemental concentrations (TM/Ca) were calculated, assuming 40 wt% for CaCO_3 .

Following data processing, rigorous screening of the Mg/Ca ratios for the influence of intratest contamination was conducted. It is important to recognize that Mn/Mg and Al/Mg of contaminant phases vary greatly, such that there is no single universal threshold for these elements that can be applied in every situation

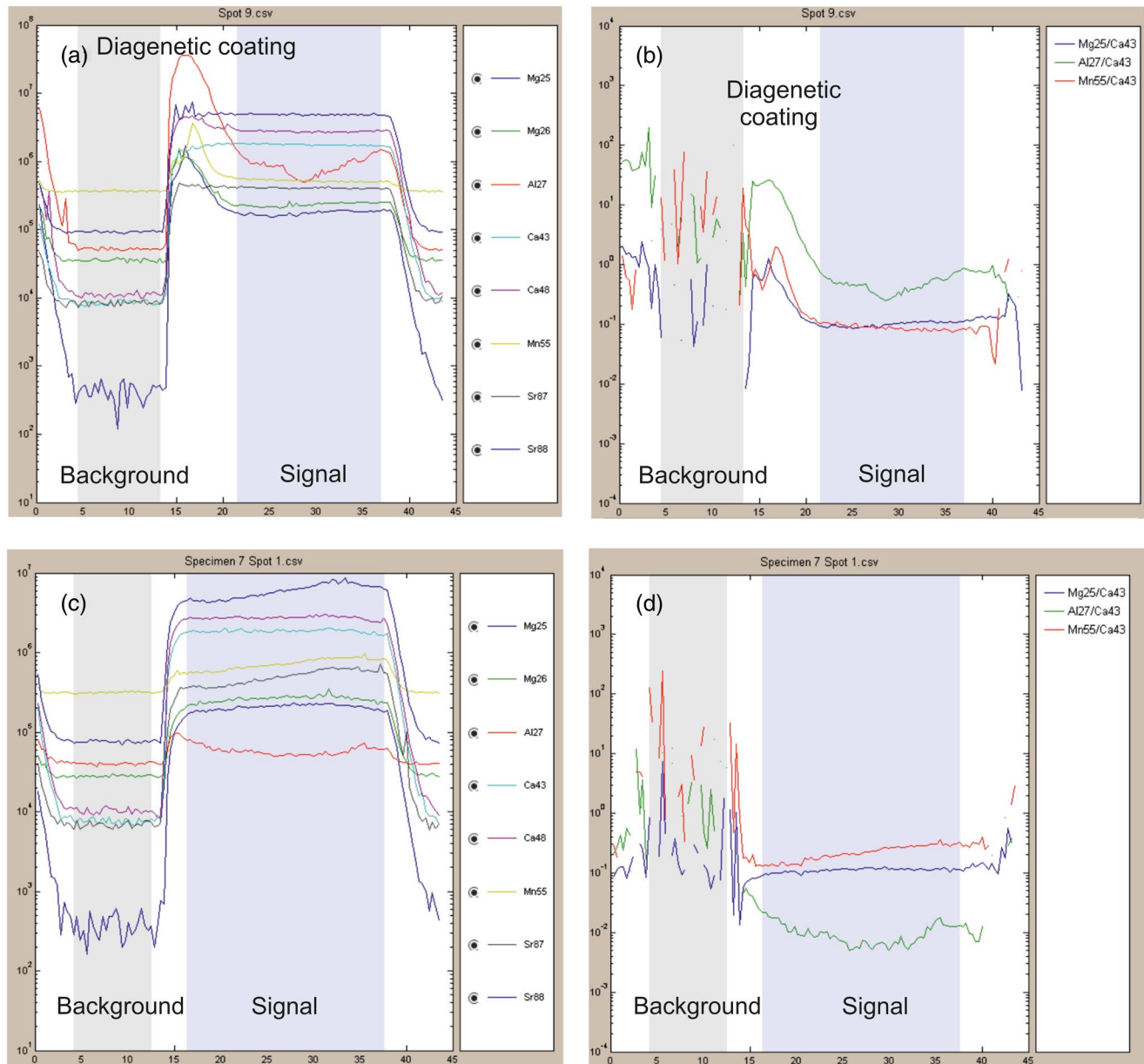


Figure 2. Representative LA-ICP-MS Mg, Al, and Mn profiles demonstrating the selection of background (gray panel) and sample (blue panel) signals for a profile with an authigenic coating (a), (b) and for a profile without an authigenic coating (c), (d). Both examples are shown in raw isotopic counts (a), (c), and ratios mode (b), (d) where the isotopes of interest are relative to ⁴³Ca, the internal standard. In both examples the x axis is analysis time (seconds), and the y axis is the raw intensity of the isotopes or ratios on a log scale. The sample interval is selected to avoid the elevated Mg/Ca, Mn/Ca, and Al/Ca at the outer surface of the test.

(Lear et al., 2015). For the Sunbird-1 samples we examined co-variation of Mg/Ca and Mn/Ca and chose to exclude all samples above a Mn/Ca threshold of 200 $\mu\text{mol/mol}$ (Figure S3). Consideration of Al/Ca was more complex, as some samples with extremely high Al/Ca (>1,000 $\mu\text{mol/mol}$) was not associated with markedly elevated Mg/Ca. This result demonstrates that aluminum is sporadically present in foraminiferal tests in variable phases (with differing Al/Mg). We therefore used a dual-pronged approach, considering both Al/Ca and intrasample heterogeneity. We excluded profiles where two conditions were met: (i) Al/Ca was >100 $\mu\text{mol/mol}$, and (ii) the associated Mg/Ca was substantially elevated relative to the other depth profiles from the same sample.

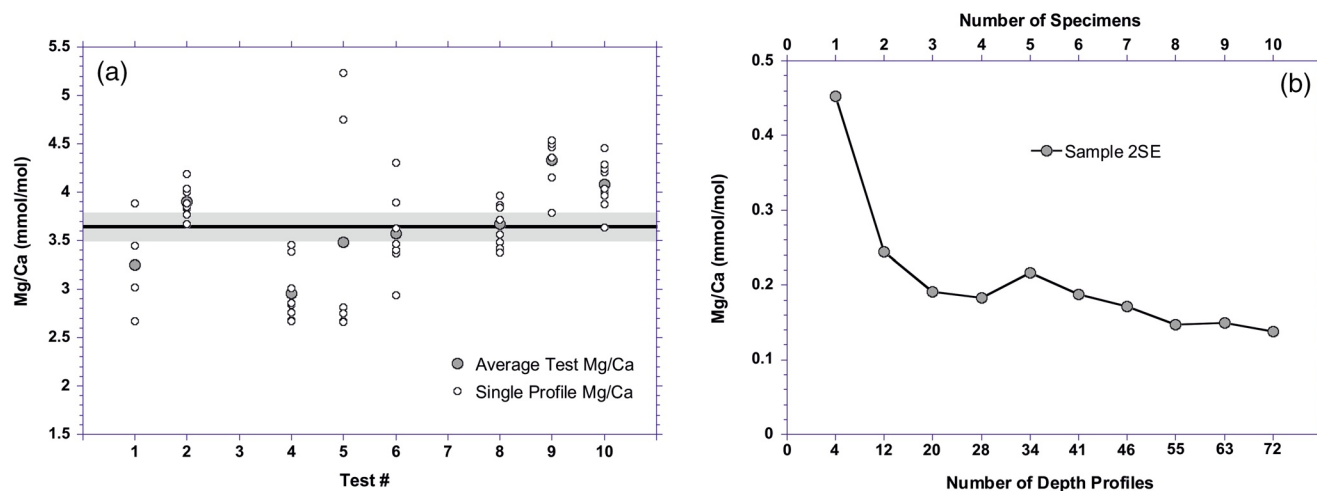


Figure 3. Distribution of *D. altispira* Mg/Ca values from LA-ICP-MS profiles of the 1,551–1,554 m sample. (a) A summary of all Mg/Ca values, where open circles denote individual measurements, and filled circles denote mean Mg/Ca values for each specimen. The horizontal black line is the mean of all depth profiles from the sample, and the gray bar the ± 2 SE sample uncertainty. (b) The evolution of the sample 2 SE with increasing specimens. Only profiles that passed data screening are included ($n = 72$). Data are provided in Table S5. ICP-MS, inductively coupled-plasma mass spectrometer.

2.6. Determination of Mean Foraminiferal Test Mg/Ca by Laser Ablation

Geochemical heterogeneity exists both within an individual foraminiferal test and between foraminiferal tests from the same sample (S. M. Eggins et al., 2004; Fehrenbacher & Martin, 2014; Sadekov et al., 2005, 2008). Therefore, several laser ablation profiles are required to produce a consistent Mg/Ca ratio for temperature reconstructions. Here we analyzed 10 depth profiles through each of 10 individual *D. altispira* tests from the 1,551–1,554 m (11.74 Ma) sample to determine representative interspecimen variability for these samples (Figure 3). Approximately one-third ($n = 28$) of the 100 depth profiles were excluded during screening for elevated Al/Ca and Mn/Ca indicative of diagenetic contamination. The Mg/Ca value of individual depth profiles in *D. altispira* from the 1,551–1,554 m sample ranges from 2.67 mmol/mol to 5.23 mmol/mol, with a mean of 3.63 ± 0.14 mmol/mol ($n = 72$) (Figure 3a; Table S5). The mean Mg/Ca value from four specimens, a total of 28 profiles, is 3.41 ± 0.18 mmol/mol (Figure 3a). Averaging profiles from 10 individual tests did therefore not produce significantly better accuracy or precision than averaging profiles from four individual tests (Figure 3b). Therefore, for a Mg/Ca ratio to be considered representative it must represent an average of at least 28 laser ablation profiles, from at least four specimens, with the analytical uncertainty (2 SE) indicating the intra and interspecimen variability this incorporates. To account for depth profiles excluded due to contamination, where possible the number of measurements per sample was increased to 36, six depth profiles per specimen and six specimens per sample. This result is in line with other LA-ICP-MS studies (Rathmann et al., 2004; A. Sadekov et al., 2008). Future studies are advised to conduct similar testing to determine the number of measurements required for a mean sample Mg/Ca to be representative, as this will likely be site dependent.

2.7. Mg/Ca Paleo-Sea Surface Temperature Calculations

The influence of calcification temperature (T) on the Mg/Ca ratio of foraminiferal calcite can be explained by an exponential curve of general form $\text{Mg/Ca} = B \exp^{AT}$ where the preexponential constant (b) and exponential constant (a) are species specific (Anand et al., 2003; Lear et al., 2002; Nürnberg et al., 1996; Rosenthal et al., 1997). To convert raw Mg/Ca ratios to absolute temperatures, several secondary controls on Mg/Ca must be considered, and accounted for (Gray et al., 2018; Holland et al., 2020; Hollis et al., 2019).

In this study we use Mg/Ca values from *D. altispira*, a near surface dweller present from the Oligocene to the Pliocene. Since this is not an extant species, we consider two approaches to calculating SST: (i) using the multispecies calibration equation from Anand et al. (2003) and (ii) using the *Globigerinoides ruber* Mg/Ca-SST equation and pH correction from Evans, Brierley, et al. (2016) and Evans, Wade, et al. (2016).

In scenario (i), we apply a compilation of nine modern planktic foraminifera (Anand et al., 2003). This calibration is commonly applied to extinct planktic foraminiferal species such as *D. altispira* and applies a power law relationship, where H is a constant that describes the sensitivity of $\text{Mg}/\text{Ca}_{\text{CALCITE}}$ to seawater Mg/Ca ($\text{Mg}/\text{Ca}_{\text{SW}}$) (Cramer et al., 2011; Evans & Müller, 2012; Hasiuk & Lohmann, 2010) (Equation 1).

$$\text{Mg} / \text{Ca} = \frac{B}{\text{Mg} / \text{Ca}_{\text{SW}}^{t=0}^H} \times \text{Mg} / \text{Ca}_{\text{SW}}^{t=H} \exp^{\text{AT}} \quad (1)$$

Fluxes of Mg^{2+} and Ca^{2+} into and out of the oceans leads to secular variation in $\text{Mg}/\text{Ca}_{\text{SW}}$. This variability must be accounted for when determining absolute sea surface temperatures on Cenozoic timescales (Hollis et al., 2019). Reconstructions of $\text{Mg}/\text{Ca}_{\text{SW}}$ based on large benthic foraminifera (Evans et al., 2018), calcite veins (Coggon et al., 2010), fluid inclusions (Horita et al., 2002), and echinoderms (Dickson, 2002) have constrained this variability through the Cenozoic (Figure S4). The Eocene-Oligocene demonstrates relatively stable values of 2.0–2.5 mol/mol (Coggon et al., 2010; Evans et al., 2018). However, only one data point exists from the Miocene, through which $\text{Mg}/\text{Ca}_{\text{SW}}$ more than doubles from ~ 2.2 mol/mol in the late Oligocene (Coggon et al., 2010) to the well constrained value of 5.2 mol/mol in the modern ocean (Broecker et al., 1982; Dickson, 2002; Horita et al., 2002; Kısakürek et al., 2008). Therefore, the method of Lear et al. (2015) is followed by fitting the fourth-order polynomial curve fit through the compiled $\text{Mg}/\text{Ca}_{\text{SW}}$ proxy records (Figure S4). We use a ± 0.5 mol/mol uncertainty window in the following temperature calculations, this error envelope incorporating the majority of the spread in the proxy data.

The power law function negates the assumption that the temperature sensitivity remains constant, independent of changing $\text{Mg}/\text{Ca}_{\text{SW}}$ through the Cenozoic era. We apply a power law constant of $H = 0.41$, similar to the value applied for *T. trilobus*, a symbiont-bearing, mixed layer dweller (Delaney et al., 1985; Evans & Müller, 2012). Adapting Equation 1 to include our H value, a modern-day $\text{Mg}/\text{Ca}_{\text{SW}}$ value of 5.2 mol/mol, and the calibration constants of Anand et al. (2003) derives Equation 2.

$$\frac{\text{Mg}}{\text{Ca}} = \frac{0.38 \pm 0.02}{5.2^{0.41}} \times \text{Mg} / \text{Ca}_{\text{SW}}^{0.41} \exp^{(0.090 \pm 0.003 \times \text{SST})} \quad (2)$$

This first calibration approach assumes that foraminiferal Mg/Ca is not influenced by changes in the carbonate system. However, studies have shown that planktic foraminiferal Mg/Ca is influenced by changes in the carbonate system, the ratio increasing with decreased pH and/or $\Delta[\text{CO}_3^{2-}]$ (Evans, Brierley, et al., 2016; Evans, Wade, et al., 2016; Gray & Evans, 2019; Gray et al., 2018; Russell et al., 2004; Yu & Elderfield, 2008). However, the ultimate driver of this effect is not certain and some species are insensitive to changes in the carbonate system. Further, it has been shown that for *Orbulina universa* dissolved inorganic carbon (DIC) plays a role in test Mg/Ca variability (Holland et al., 2020). We follow recent results which interpret pH, as opposed to $\Delta[\text{CO}_3^{2-}]$ or DIC, as the parameter which controls the carbonate system's influence on Mg/Ca (Evans, Brierley, et al., 2016; Evans, Wade, et al., 2016; Gray et al., 2018). Furthermore, unlike with either DIC or $\Delta[\text{CO}_3^{2-}]$, it is possible to reconstruct pH through the Neogene using boron isotopes in foraminifera (Foster & Rae, 2015; Greenop et al., 2014; Henahan et al., 2013; Sosdian et al., 2018). For these reasons we use the recent Neogene boron isotope compilation of Sosdian et al. (2018), which provides well constrained estimates of pH across this time interval (Figure S5; Table S9). Linear interpolation between these pH values allows us to estimate a mean pH value, and associated uncertainty envelope, for each Sunbird-1 sample, where the uncertainty envelope is maximum and minimum pH at the 17% and 83% confidence interval ($\sim \pm 0.06$ pH units).

Therefore, in addition to scenario (i) we also consider the approach from Evans, Brierley, et al. (2016) and Evans, Wade, et al. (2016) which corrects for pH changes using the interpolated Neogene pH record of Sosdian et al. (2018) (Figure S5). Measured planktic foraminiferal Mg/Ca values are corrected for this influence of pH using the equation of Evans, Brierley, et al. (2016) and Evans, Wade, et al. (2016) (Equation 3).

$$\text{Mg} / \text{Ca}_{\text{CORRECTED}} = \frac{\text{Mg} / \text{Ca}_{\text{MEASURED}}}{\frac{0.66}{1 + \exp(6.9(\text{pH} - 8.0))} + 0.76} \quad (3)$$

The preferred equation of Evans, Brierley, et al. (2016) and Evans, Wade, et al. (2016) is used to account for the influence of changing Mg/Ca_{sw} when estimating SST. These authors determined that the best fit to culture-derived calibration lines is when both the preexponential (b) and exponential (a) coefficients vary quadratically with Mg/Ca_{sw} (Equations 4 and 5).

$$B = \left(0.019 \times Mg / Ca_{sw}^2\right) - \left(0.16 \times Mg / Ca_{sw}\right) + 0.804 \quad (4)$$

$$A = \left(-0.0029 \times Mg / Ca_{sw}^2\right) + \left(0.032 \times Mg / Ca_{sw}\right) \quad (5)$$

We substitute these equations into the general exponential calibration, $Mg/Ca = Bexp^{AT}$, to account for changing Mg/Ca_{sw} . Although the Evans, Brierley, et al. (2016) and Evans, Wade, et al. (2016) equation is specific to *G. ruber*, this species inhabits a shallow water depth of 0–50m (Schiebel & Hemleben, 2017) similar to the inferred mixed-layer habitat depth *D. altispira* (Aze et al., 2011). Furthermore, as with *G. ruber*, *D. altispira* was a tropical/subtropical species, with symbionts (Aze et al., 2011).

Salinity can exert a secondary effect on foraminiferal Mg/Ca , sensitivity measurements from culture and core-top studies show this to be $\sim 3\text{--}5\%$ per practical salinity unit (psu) (Gray et al., 2018; Hollis et al., 2019; Hönisch et al., 2013; Kısakürek et al., 2008). In the absence of a robust, independent salinity proxy (although we do note the promise of Na/Ca [Bertlich et al., 2018; Geerken et al., 2018]) and the relatively minor effect of salinity on foraminiferal Mg/Ca , this potential secondary control is not empirically accounted for. Sunbird-1 was located in a coastal setting and likely experienced a highly variable hydrological cycle due to changes in the position of the ITCZ making it susceptible to changes in salinity. Therefore, an error of $\pm 0.5^\circ\text{C}$ is incorporated into the final sea surface temperature estimates, equivalent to an assumed salinity variability of $\sim \pm 1$ PSU.

Mg/Ca -derived sea surface temperature estimates calculated using both approaches (i) and (ii) yield extremely similar trends (Figure S6). Across the time interval of the Sunbird-1 data set ($\sim 13.5\text{--}9.5$ Ma) pH changes by a small amount and thus the choice of approach has little influence on the Sunbird-1 absolute SST record. In our discussion below, we adopt approach (i); the multispecies calibration equation from Anand et al. (2003) without a pH correction. This approach avoids any potential species-specific effects from applying the Evans, Brierley, et al. (2016) and Evans, Wade, et al. (2016) calibration specific to *G. ruber* to the extinct *D. altispira* used in this study. Furthermore, *D. altispira* has been considered to be symbiont bearing, so may demonstrate a muted response to changes in pH and insensitivity to pH changes, similar to *Trilobatus trilobus* (Gray & Evans, 2019).

The uncertainties ($\pm 2SE$) associated with the conversion from Mg/Ca to absolute SST estimates incorporate the uncertainty on the Mg/Ca_{sw} record, and the potential uncertainty due to varying salinity. Additionally, scenario (i) incorporates the uncertainty in the calibration of Anand et al. (2003) (Equation 2), and scenario (ii) using the approach of Evans, Brierley, et al. (2016) and Evans, Wade, et al. (2016) incorporates the uncertainty in the pH correction. These combined are termed the calibration uncertainty and are considerably greater than the independent analytical uncertainty, which only incorporates the intra and interspecimen variability (± 2 SE). Absolute sea surface temperature estimates, and associated uncertainties, calculated using approach (i) and (ii) are available in Table 1 and Table S9 respectively

2.8. $\delta^{18}\text{O}$ Paleo-Sea Surface Temperature Calculations

Due to the limited sampling resolution of the trace metal data, SST is also calculated using foraminiferal $\delta^{18}\text{O}$. Foraminiferal $\delta^{18}\text{O}$ ($\delta^{18}\text{O}_{\text{calcite}}$) is converted to temperature (T) using the palaeotemperature equation of Bemis et al. (1998) (Equation 6), changes in global ice volume being corrected using the $\delta^{18}\text{O}_{sw}$ value from the nearest 0.1 Myr time interval in the compilation of Cramer et al. (2011).

$$\left(\delta^{18}\text{O}_{\text{calcite}} - \delta^{18}\text{O}_{sw} + 0.27\right) = -0.21 \pm 0.003T + 3.10 \pm 0.07 \quad (6)$$

Table 1

Sunbird-1 LA-ICP-MS Mg/Ca Derived SST Using the Approach of Anand et al. (2003) Without a pH Correction

Age (Ma)	Minimum age (Ma)	Maximum age (Ma)	Temperature (°C)	Maximum temperature (°C)	Minimum temperature (°C)	Analytical error only maximum temperature (°C)	Analytical error only minimum temperature (°C)
9.53	9.43	9.62	27.73	31.08	24.64	28.30	27.12
9.86	9.86	9.86	28.15	31.86	24.68	29.06	27.17
10.19	10.05	10.33	29.54	33.49	25.81	30.62	28.34
10.43	10.43	10.43	26.82	30.55	23.32	27.78	25.77
10.48	10.48	10.48	28.13	31.58	24.94	28.77	27.44
10.57	10.57	10.57	27.81	31.47	24.41	28.66	26.90
10.62	10.62	10.62	24.88	28.12	21.90	25.43	24.30
10.78	10.73	10.89	29.48	33.14	26.09	30.27	28.64
10.92	10.92	10.92	28.95	32.78	25.36	29.92	27.89
11.13	10.98	11.28	28.42	32.47	24.58	29.61	27.09
11.40	11.40	11.40	28.18	31.50	25.15	28.67	27.68
11.50	11.46	11.55	29.36	32.85	26.15	29.98	28.71
11.61	11.10	11.61	26.78	30.39	23.44	27.59	25.91
11.63	11.63	11.63	26.65	30.34	23.21	27.55	25.68
11.64	11.64	11.64	29.57	33.29	26.11	30.40	28.68
11.67	11.67	11.67	25.44	29.02	22.12	26.26	24.55
11.72	11.69	11.74	28.19	31.84	24.81	28.99	27.33
11.77	11.77	11.77	26.89	30.09	23.96	27.30	26.46
11.82	11.82	11.82	26.39	29.69	23.37	26.92	25.85
11.87	11.87	11.87	28.84	32.47	25.47	29.60	28.02
12.03	12.03	12.03	28.10	31.66	24.82	28.81	27.35
12.71	12.57	12.85	29.14	32.80	25.77	29.90	28.34
13.23	13.13	13.33	28.85	32.54	25.43	29.64	28.00

Abbreviations: LA-ICP-MS, laser ablation-inductively coupled-plasma mass spectrometer; SST, sea surface temperature.

Notes. Minimum and maximum age refer to the age range of the pooled samples (Table S7). Maximum and Minimum temperatures refer to the full range of absolute temperatures derived incorporating the analytical and calibration uncertainty, whereas Analytical Error Only Maximum and Minimum temperatures refer to the range of temperatures derived from the analytical uncertainty only.

The absence of a robust, independent salinity proxy makes any quantitative attribution of its influence on foraminiferal $\delta^{18}\text{O}$ challenging. Therefore, we incorporate potential $\delta^{18}\text{O}$ variability due to salinity into any temperature estimate uncertainty. Salinity of the upper water column in a $0.75^\circ \times 0.75^\circ$ grid square around the modern-day study site varies between 34.9 and 35.4 PSU (Boyer et al., 2013). Using the Indian Ocean $\delta^{18}\text{O}_{\text{sw}}$ -salinity relationship of LeGrande and Schmidt (2006) (Equation 7) this equates to a maximum $\delta^{18}\text{O}_{\text{sw}}$ uncertainty of $\pm 0.091\text{‰}$. Using Equation 6 this equates to a 0.4°C uncertainty in the calculated surface temperature.

$$\delta^{18}\text{O}_{\text{sw}}(\text{SMOW}) = (0.16 \pm 0.004 \times \text{Salinity}) - 5.31 \pm 0.135 \quad (7)$$

We acknowledge the likelihood of variability in sea surface salinity in this downcore record. We use the paleolatitude calculator of van Hinsbergen et al. (2015) to calculate a paleolatitude for Sunbird-1 at 10 Ma of approximately 5.5°S . The latitudinal correction of Zachos et al. (1994) gives a $\delta^{18}\text{O}_{\text{sw}}$ of 0.1‰ . The absence of a significant offset from SMOW (0‰) suggests that this will have a negligible influence on the isotopic SST reconstructions.

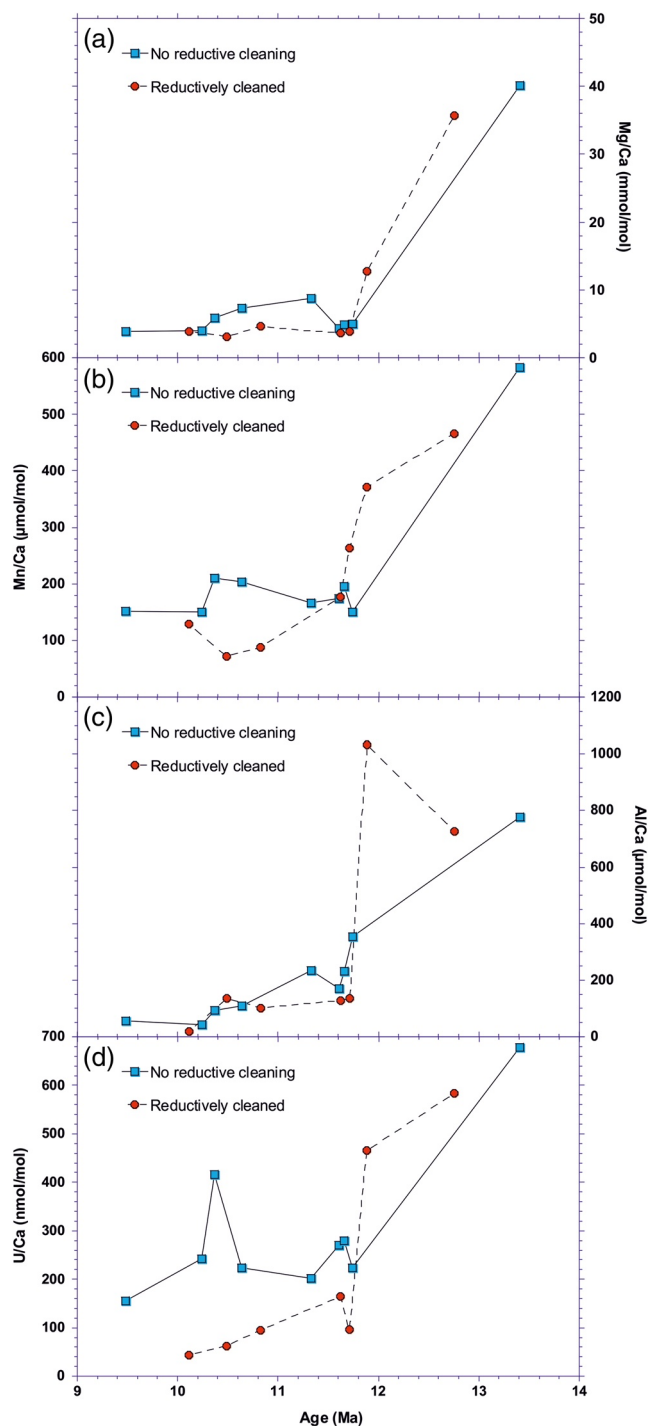


Figure 4. Downcore solution ICP-MS (a) Mg/Ca, (b) Mn/Ca, (c) U/Ca, and (d) Al/Ca records for *D. altispira* in the Sunbird-1 core, distinguishing between sample that were reductively cleaned (red circles) and those that were not (blue squares).

3. Results

3.1. Solution ICP-MS Trace Element Chemistry

D. altispira Mg/Ca measured by solution ICP-MS ranges from 3.15 ± 0.1 to 40.2 ± 0.2 mmol/mol (Figure 4a), translating to unrealistically high reconstructed sea surface temperatures. The high Mg/Ca ratios strongly suggest the addition of magnesium from a secondary, postdepositional source, prior to 11.75 Ma. The elevated Mg/Ca ratios are associated with correspondingly high Mn/Ca, Al/Ca, and U/Ca (Figures 4b–4d). Six of the 16 Mn/Ca ratios are in excess of the proposed 200 $\mu\text{mol/mol}$ threshold, from our LA-ICP-MS analysis, above which Mg/Ca ratios are excluded due to contamination (Figure S3). Furthermore, every foraminiferal U/Ca ratio is considerably higher than typical U/Ca ratios of primary foraminiferal calcite, which range from ~ 3 to 23 nmol/mol (Chen et al., 2017; Raitzsch et al., 2011; Russell et al., 2004). In addition, foraminiferal Al/Ca exceeds the commonly applied 100 $\mu\text{mol/mol}$ threshold in all but the four youngest samples.

The presence of elevated foraminiferal Mn/Ca, Al/Ca, and U/Ca ratios does not necessarily mean that the Mg/Ca ratios are contaminated. However, the downcore, point to point correlation (Figure 4) and covariance (Figure S7) between Mg/Ca and contaminant indicators suggest a strong association. This downcore association between Mg/Ca and contaminant indicators, despite a rigorous chemical cleaning protocol, suggests one of two things; (i) the chemical cleaning protocol is not fully effective at removing contaminant coatings, and/or (ii) an Mg-rich contaminant phase is pervasive throughout the calcite test.

Including the reductive cleaning step lowers Mg/Ca, Mn/Ca, and U/Ca ratios in the post 11.8 Ma portion of the record, but has a negligible effect on Al/Ca. Neither cleaning protocol is effective at removing the authigenic coatings on the Sunbird-1 foraminifera in the pre 11.8 Ma portion of the record (Figure 4). For this reason, we also analyzed Sunbird-1 planktic foraminifera by laser ablation ICP-MS.

3.2. Downcore Laser Ablation ICP-MS Mg/Ca

Our laser ablation profiles clearly demonstrate that the metal-rich contaminant is present as an authigenic surface coating on the glassy foraminifera (e.g., Figures 2a and 2b). Because the alteration is not pervasive throughout the calcite test, laser ablation ICP-MS is an ideal approach to determine primary test Mg/Ca on these coated samples (Section 2.6). *D. altispira* Mg/Ca determined by laser-ablation ICP-MS ranges from 3.03 to 5.07 mmol/mol, with an average value of 4.18 ± 0.40 mmol/mol, and errors ($\pm 2\text{SE}$) range from 0.10 to 1.04 mmol/mol (Table S6). However, due to elevated Al/Ca and Mn/Ca ratios, only 14 of the 44 samples are represented by at least 28 laser profiles. To alleviate this problem, adjacent samples have been combined into longer time slices to ensure that the absolute mean Mg/Ca measurements are robust (Table S7). Samples comprising the mean of at least 28 laser profiles are termed “unpooled samples.” Samples pooled to achieve a minimum of 28 laser profiles are termed “pooled samples.” It is acknowledged that combining adjacent

samples, which span up to 420 kyr, could incorporate orbital scale climatic variability into these pooled samples. However, we do not infer climatic variability on orbital timescales because the coarse sampling resolution could incorporate aliasing of any precessional or obliquity periodicity into longer term eccentricity

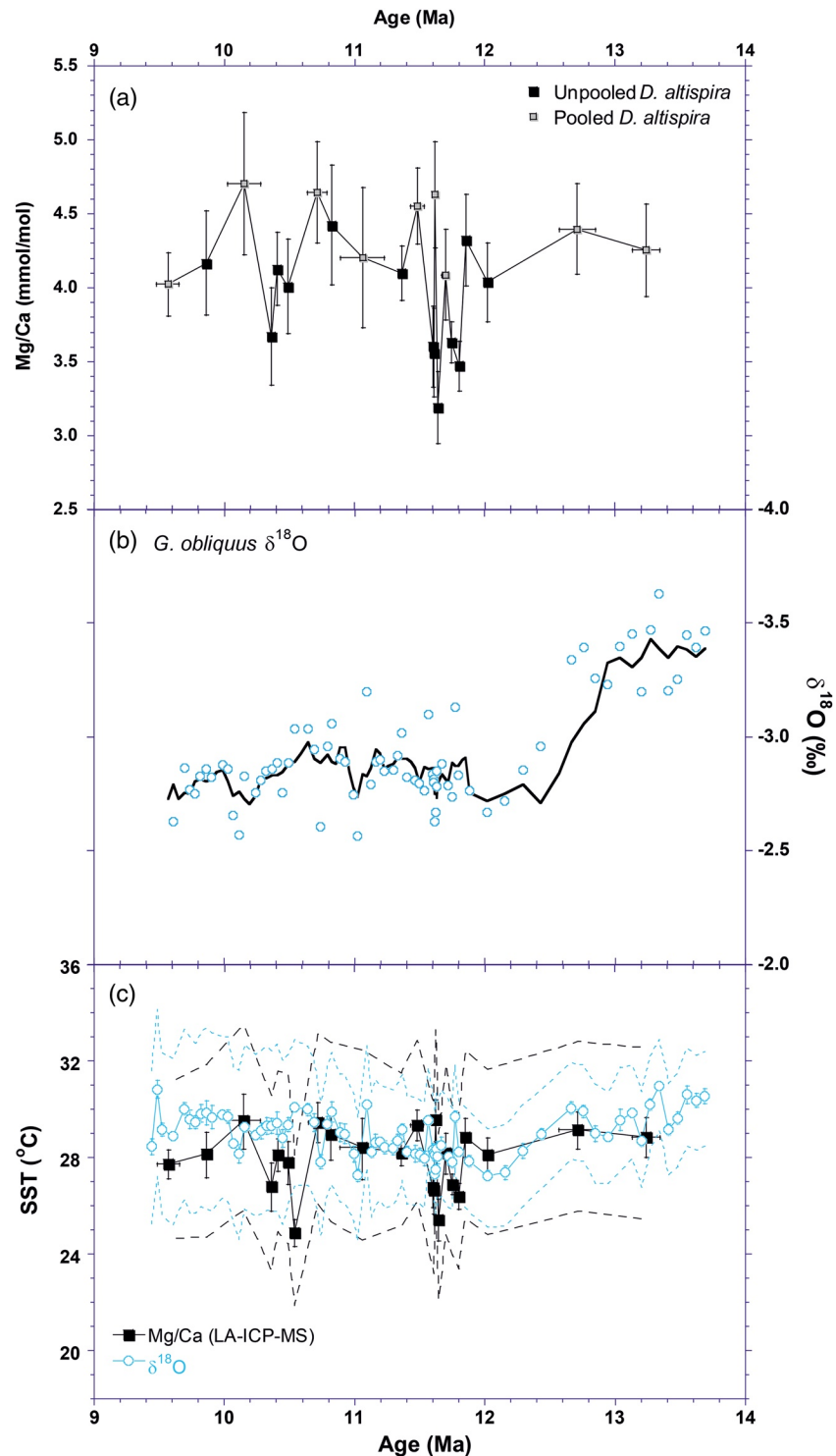


Figure 5. (a) Mean *D. altispira* LA-ICP-MS Mg/Ca ratios (mmol/mol) for unpooled (black squares) and pooled (gray squares) samples from Sunbird-1. Error bars denote the age range for pooled samples, and the ± 2 SE of Mg/Ca from all depth profiles in the sample. (b) *G. obliquus* $\delta^{18}\text{O}$ from Sunbird-1. Solid line is a five-point moving average. (c) Sea surface temperature records at Sunbird-1 from planktic foraminiferal $\delta^{18}\text{O}$, and LA-ICP-MS Mg/Ca using our preferred approach that applies the calibration of Anand et al. (2003) without a pH correction. Symbols are the same as in (a) and (b). Error bars on the $\delta^{18}\text{O}$ record denote the analytical uncertainty (± 2 SD), and error bars on the Mg/Ca record denote the sample uncertainty (± 2 SE). As in (a), pooled Mg/Ca samples also have horizontal error bars denoting the sample age range. Dashed blue and black lines denote the full uncertainty on the temperature estimates, including that derived from the calibration uncertainty, for $\delta^{18}\text{O}$ and LA-ICP-MS Mg/Ca respectively. Figure S8 provides LA-ICP-MS Mg/Ca sea surface temperatures using the alternative approach of Evans, Brierley, et al. (2016) and Evans, Wade, et al. (2016). ICP-MS, inductively coupled-plasma mass spectrometer.

cycles (Pisias & Mix, 1988). Combining adjacent samples to generate a representative mean Mg/Ca for a longer time-slice could smooth orbital scale variability, could reduce uncertainty and assist the interpretation of longer-term climatic trends.

The mean Mg/Ca of representative samples after incorporating the nine pooled Mg/Ca samples with the 14 unpooled samples ranges from 3.08 to 4.70 mmol/mol, with an average value of 4.04 ± 0.29 mmol/mol, and errors ($\pm 2SE$) range from 0.14 to 0.48 mmol/mol (Table S8). These values are in good agreement with the reductively cleaned solution ICP-MS data for the post-11.8 Ma portion of the record (Figure S2), coinciding with the interval when contaminant indicators (Mn/Ca, Al/Ca, and U/Ca) are substantially lower (Figures 4b–4d). This agreement between Mg/Ca values obtained by LA-ICP-MS and solution ICP-MS following effective reductive-cleaning supports the suitability of the LA-ICP-MS analyses. Because we can be more confident that the laser ablation data are not biased by authigenic coatings, the laser-ablation approach has the advantage that we can also determine original test Mg/Ca in the older part of the record.

There is no obvious long-term trend in Mg/Ca through the interval (Figure 5a). Between 11.8 Ma and 11.7 Ma there is a 0.7–0.8 mmol/mol decrease in Mg/Ca followed by a recovery to approximately previous values at 11.5–11.4 Ma. There is a Mg/Ca decrease of similar magnitude from between 10.7 Ma and 10.36 Ma, recovering by 9.85 Ma. We acknowledge that the coarse sampling frequency, and the combining of samples could be obscuring similar variability through the rest of the record.

3.3. *G. obliquus* $\delta^{18}O$

G. obliquus $\delta^{18}O$ ranges from -3.63‰ to -2.34‰ with a mean value of -2.92‰ . The $\delta^{18}O$ record shows very little variability, values remaining stable at -3.4‰ prior to a positive 0.6‰ shift at ~ 12.5 Ma, and -2.7‰ after (Figure 5b). The low variability translates to a stable $\delta^{18}O$ SST record, temperatures ranging between $27^{\circ}C$ and $31^{\circ}C$ with the only distinctive trend being a $\sim 3^{\circ}C$ decrease between ~ 12.7 Ma and 12.0 Ma. The coeval positive 0.3‰ shift in seawater $\delta^{18}O$ (Cramer et al., 2011) dampens the influence on the SST estimate of the positive 0.6‰ shift in *G. obliquus* $\delta^{18}O$ at ~ 12.5 Ma.

4. Discussion

4.1. Reconstructing Sea Surface Temperature From Diagenetically Altered Foraminifera Using Laser Ablation ICP-MS

Robust paleotemperature reconstructions using foraminiferal Mg/Ca ratios are reliant upon the Mg/Ca ratio recording a primary environmental signal, unaltered by diagenetic alteration. Despite employing a thorough cleaning protocol (Barker et al., 2003; Boyle & Keigwin, 1985), our Mg/Ca ratios from solution-based ICP-MS analysis in the >11.8 Ma portion of the record are clearly influenced by a diagenetic contaminant phase containing elevated magnesium (Figure 4). This finding demonstrates that foraminifera with a glassy appearance under the light microscope are not necessarily free from the influence of all modes of diagenetic alteration. We therefore emphasize the importance of complementary trace metal ratios indicative of contamination (i.e., Al/Ca, Mn/Ca, U/Ca) to assess the reliability of foraminiferal Mg/Ca ratios (Figure 4). The application of LA-ICP-MS to collect high resolution elemental profiles through the foraminiferal tests, excluding regions displaying diagenetic contamination, has facilitated the identification of what we interpret to be primary paleotemperatures from diagenetically altered foraminifera (Hines et al., 2017; Hollis et al., 2015).

The Sunbird-1 $\delta^{18}O_{PF}$ SST record from *G. obliquus* reconstructs very similar absolute temperatures to the planktic foraminiferal Mg/Ca SST record (Figure 5c). Mean SST from the Sunbird-1 $\delta^{18}O_{PF}$ record ($29^{\circ}C$) is $2^{\circ}C$ higher than mean SST from the Mg/Ca record ($27^{\circ}C$), although with the exception of the two transient decreases in Mg/Ca reconstructed SST initiating at 11.8 and 10.7 Ma the records are within error. The similarity of the absolute SSTs reconstructed by the two proxies strengthens the case for the LA-ICP-MS Mg/Ca SST record recording a primary temperature signal, and that these absolute sea surface temperatures at Sunbird-1 should be considered primary.

The majority of the uncertainty in the absolute temperature estimates is derived from the uncertainties incorporated from the relevant calibrations, in particular the seawater Mg/Ca and seawater $\delta^{18}O$ records

(Figure 5c). This is true for both LA-ICP-MS Mg/Ca (Table 1 and Table S9) and $\delta^{18}\text{O}$ (Table S10). Therefore, despite being appreciable, the uncertainty resulting from the geochemical heterogeneity both within an individual foraminiferal test and between foraminiferal tests from the same sample (Figure 3) is not the primary contributor to the final absolute temperature uncertainty.

4.2. Mid-Late Miocene Sea Surface Temperatures in the Equatorial Indian Ocean

The results from Sunbird-1 indicate that SST in the equatorial Indian Ocean remained stable at $\sim 27^{\circ}\text{C}$ – 29°C through the 13.3 to 9.5 Ma interval (Figure 5c). This finding suggests that tropical climate was relatively stable following the global cooling associated with the expansion of the East Antarctic Ice Sheet across the MMCT. These records from Sunbird-1 supports the robustness of contemporaneous alkenone based studies which exhibit similar absolute tropical SST estimates (Herbert et al., 2016; Huang et al., 2007; Rousselle et al., 2013; Seki et al., 2012; Zhang et al., 2014) (Figure 6a). The U^{k}_{37} SST calibration fails to reconstruct $\text{SST} > 29^{\circ}\text{C}$ (Müller et al., 1998) but these results using Mg/Ca paleo-thermometry suggest that outside the western Pacific warm pool this restriction does not apply to this time interval, unlike the preceding MCO during which Mg/Ca temperature estimates are higher than those estimated with the U^{k}_{37} proxy (Badger et al., 2013).

Although not a true tropical location, and consisting of only three data points, the Badger et al. (2013) Mg/Ca record from the Mediterranean estimates SST of $\sim 27.5^{\circ}\text{C}$ between 13.5 and 13 Ma, within the Sunbird-1 SST uncertainty envelope (Figure 6b). Mg/Ca-SST records based on less well-preserved planktic foraminifera also suggest stable tropical SST between 13.8 and 11.4 Ma (Sosdian & Lear, 2020) (Figure 6b). Furthermore, well preserved planktic foraminifera from clay-rich sediments of coastal Tanzania yield Indian Ocean sea surface temperatures of 27°C at 12.2 Ma and 29°C at 11.55 Ma using the $\delta^{18}\text{O}$ paleo-thermometer (Stewart et al., 2004), again in agreement with the Sunbird-1 temperature estimates (Figure 6b). It is worth noting that this study, as well as the tropical SST records of Herbert et al. (2016) and references therein, do not sample the warm pool of the Western Pacific. Sea surface temperature estimates for the western equatorial Pacific using the TEX_{86} paleothermometer suggest a slight, $\sim 1^{\circ}\text{C}$, SST decrease between 12 and 9 Ma, while those for the eastern equatorial Pacific are more or less constant across the same interval (Zhang et al., 2014).

Although the estimates provided by the Sunbird-1 record suggest absolute tropical sea surface temperatures remained relatively stable through the mid-late Miocene, some temporal variability does persist. Between 11.8 and 11.7 Ma SST drops sharply by $\sim 3^{\circ}\text{C}$. Excluding one value of 28.6°C at 11.62 Ma, this decrease in SST to ~ 24 – 25°C persists for ~ 300 kyr before recovering to pre excursion values by 11.5 Ma. However, no transient decrease in sea surface temperature is recorded from contemporaneous alkenone based estimates of tropical SST utilizing the U^{k}_{37} proxy from the Arabian Sea (Huang et al., 2007), and the Eastern Equatorial Pacific (Herbert et al., 2016; Rousselle et al., 2013; Seki et al., 2012; Zhang et al., 2014) (Figure 6a). We therefore suggest that the observed transient $\sim 3^{\circ}\text{C}$ SST decrease is not the result of a global driver, and supports a mechanism causing local ocean cooling of the surface waters at Sunbird-1. An alternative hypothesis is that an unaccounted increase in local salinity and/or pH, lowering foraminiferal Mg/Ca ratios, caused a bias to cooler temperatures between ~ 11.8 and 11.5 Ma. Assuming constant SST, the observed ~ 0.7 mmol/mol decrease in Mg/Ca would require a salinity increase on the order of 5.0 PSU (Gray et al., 2018; Hönisch et al., 2013). This salinity increase equates to a 0.8 ‰ change in $\delta^{18}\text{O}$ using the Indian Ocean $\delta^{18}\text{O}_{\text{sw}}$ -salinity relationship of LeGrande and Schmidt (2006) (Equation 5). As well as being an extremely large change in salinity, the planktic foraminiferal $\delta^{18}\text{O}$ record does not support such a significant change in sea surface salinity between ~ 11.8 and 11.5 Ma (Figure 5b). However, we do acknowledge that a contribution from increased salinity control cannot be discounted. Despite incorporating varying pH from a globally distributed set of open ocean sites (Sosdian et al., 2018), a localized increase in pH at Sunbird-1 cannot be ruled out. This possibility may be particularly relevant considering the land-proximal, tectonically active nature of the study site. A further possibility is that selective dissolution of foraminiferal chambers precipitated during warmer seasons occurred during postburial diagenetic alteration, causing an apparent $\sim 3^{\circ}\text{C}$ lowering of SST between 11.8 and 11.5 Ma. However, mean *D. altispira* test weights suggest that there was no increased dissolution of the foraminiferal tests through this interval of lower LA-ICP-MS Mg/Ca derived SST (Table S11 and Figure S10).

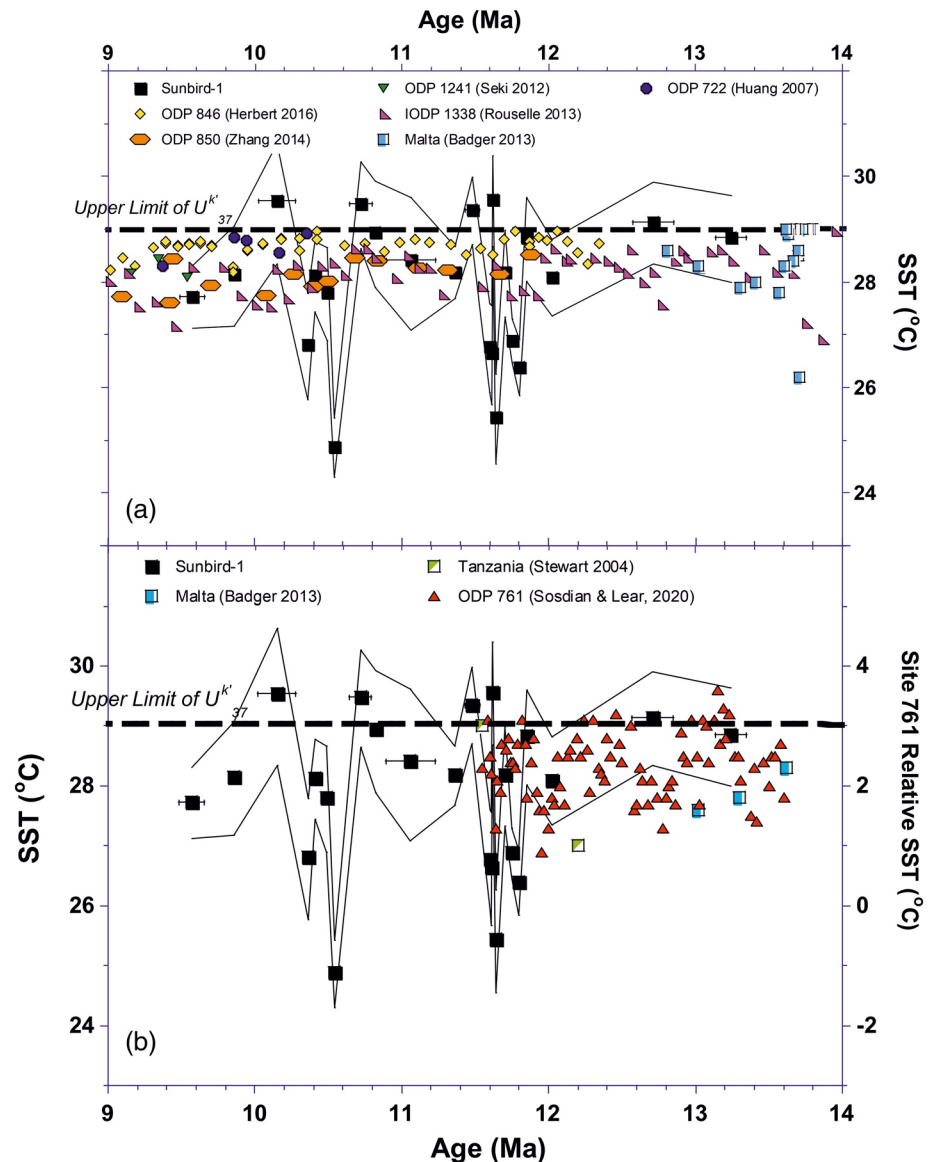


Figure 6. Sunbird-1 LA-ICP-MS Mg/Ca derived SST using the approach of Anand et al. (2003) without a pH correction compared to and SST estimates at contemporaneous sites from (a) U^{k}_{37} , and (b) foraminiferal geochemistry. Estimates applying U^{k}_{37} are from ODP Site 722 (Huang et al., 2007) in the Arabian Sea, ODP & IODP Sites 846 (Herbert et al., 2016), 850 (Zhang et al., 2014), 1,241 (Seki et al., 2012), and U1338 (Rousselle et al., 2013) in the Eastern Equatorial Pacific, terrestrial outcrops in Malta (Badger et al., 2013). Estimates applying the foraminiferal Mg/Ca proxy are from ODP Sites 761 (Sosdian and Lear, 2020) and terrestrial outcrops in Malta (Badger et al., 2013). ODP Site 761 data are displayed on an alternative axis as SST anomalies relative to the baseline average from 16.0 to 15.5 Ma. Two temperature estimates using the $\delta^{18}O$ of exceptionally preserved foraminifera from Tanzania are also shown (Stewart et al., 2004). The upper limit for the U^{k}_{37} proxy (29°C) is marked by the thick dashed black line. All previously published records used for comparison are kept on their original age models. Figure S9 provides LA-ICP-MS Mg/Ca sea surface temperatures using the alternative approach of Evans, Brierley, et al. (2016) and Evans, Wade, et al. (2016). ICP-MS, inductively coupled-plasma mass spectrometer; SST, sea surface temperature.

Therefore, our preferred interpretation is for a local cooling between ~ 11.8 and 11.5 Ma. The lack of a marked increase in the planktic $\delta^{18}O$ record at this time implies that the cooling was associated with a freshening of surface waters (Figure 5c). Interestingly, this interval corresponds to a period of very high sedimentation rates (Figure S1), which might be consistent with enhanced precipitation and runoff, lowering regional surface salinity.

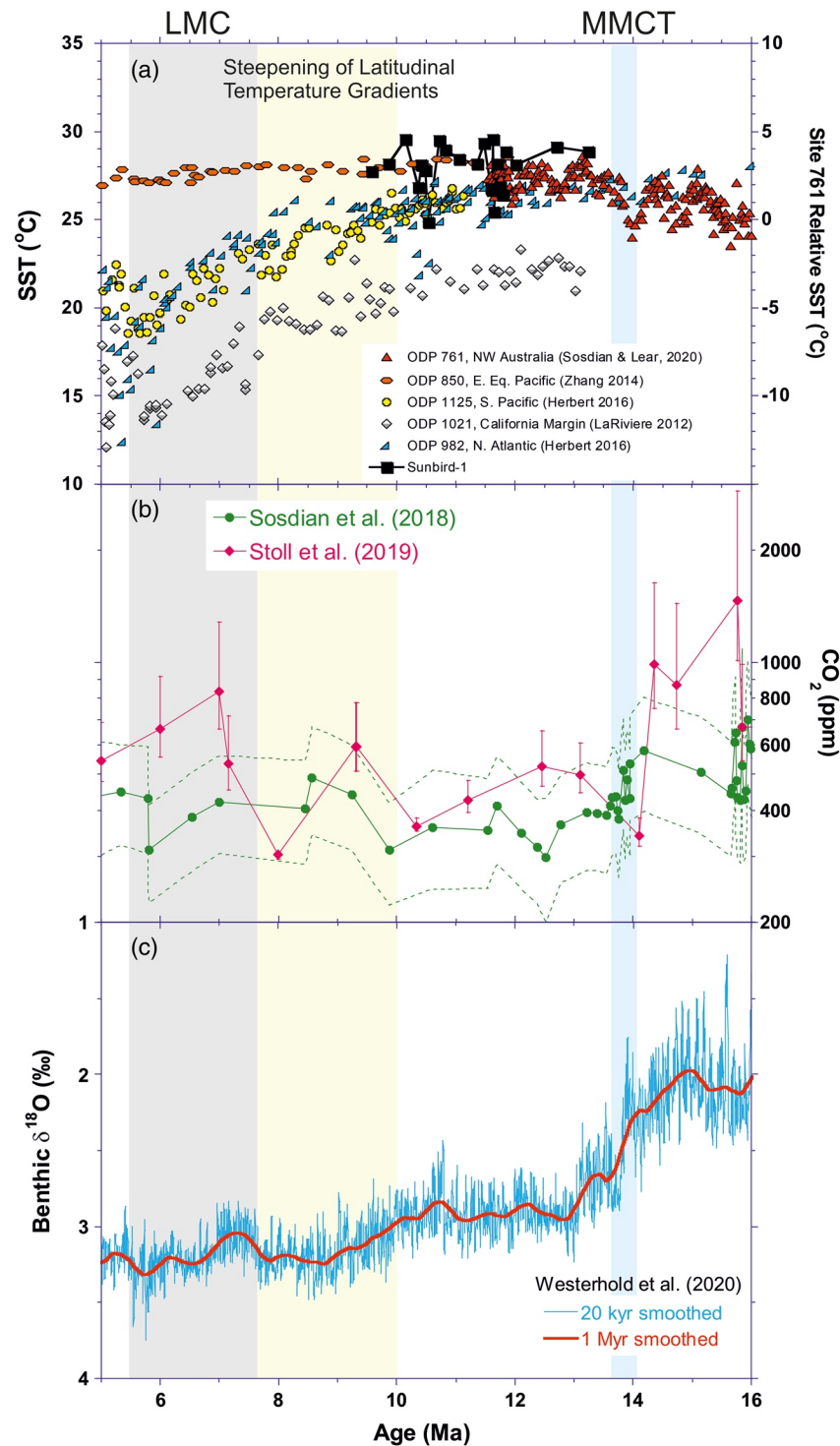


Figure 7. Summary of global climate through the mid-to-late Miocene. (a) Sea surface temperature estimates from Sunbird-1, fellow low latitude ODP sites 850 (Zhang et al., 2014) and 761 (Sosdian & Lear, 2020), mid latitude Northern Hemisphere ODP site 1,021 (LaRiviere et al., 2012), and mid-latitude Southern Hemisphere site 1,125 (Herbert et al., 2016), and high-latitude Northern Hemisphere ODP Site 982 (Herbert et al., 2016). ODP Site 761 data are displayed on an alternative axis as SST anomalies relative to the baseline average from 16.0 to 15.5 Ma. (b) pCO₂ reconstructions, with Y axis on a log scale, of Sosdian et al. (2018) applying the CCD reconstruction of Pálike et al. (2012) and the δ¹¹B_{SW} scenario of Greenop et al. (2017), and Stoll et al. (2019) applying temperature estimates from Bolton et al. (2016) and Zhang et al. (2013). Confidence intervals (95%) are displayed as dashed lines and error bars respectively. (c) Composite benthic δ¹⁸O record showing data that have been smoothed by a locally weighted function over 20 kyr (blue curve) and 1 Myr (red curve) (Westerhold et al., 2020). Blue, yellow, and gray panels indicate intervals of ice sheet expansion across the Mid Miocene Climate Transition (MMCT) associated with CO₂ decline, the steepening of latitudinal temperature gradeints in the absence of a CO₂ trend, and the Late Miocene Cooling (LMC). SST, sea surface temperature.

4.3. Implications for the Global Climate State during the Mid-late Miocene

Previous studies utilizing the U^{k}_{37} proxy suggest a substantial cooling of sea surface temperature at mid-to-high latitudes in both hemispheres between 10 and 5.5 Ma, while tropical sea surface temperatures show limited cooling in the late Miocene prior to ~7 Ma (Herbert et al., 2016; LaRiviere et al., 2012). The absolute tropical SST record reported in this study supports the finding that the latitudinal temperature gradient steepened from ~10 Ma, as the climate system transitioned toward its modern-day state. , support for the absolute temperatures reconstructed by the alkenone proxy suggests that the interval between 10 and 7.5 Ma was associated with enhanced polar amplification, significantly greater than that calculated for the greenhouse climate of the Eocene (Cramwinckel et al., 2018). There is little evidence for a significant change in pCO_2 in this interval (Sosdian et al., 2018; Stoll et al., 2019) (Figure 7). We speculate that the marked regional cooling between 10 and 7.5 Ma perhaps reflects processes internal to the climate system, involving for example ocean-atmospheric heat transport, sea ice extent, or changes in regional cloud cover. A combined data-modeling approach would help constrain possible factors and explore potential relationships between this highly heterogeneous cooling and the CO_2 drawdown that was associated with the subsequent global late Miocene Cooling starting ~7.5 Ma (Figure 7).

5. Conclusions

Our Sunbird-1 sea surface temperature estimates from LA-ICP-MS Mg/Ca analyses are in good agreement with those using the $\delta^{18}O$ paleo-thermometer on glassy foraminifera, supporting the use of LA-ICP-MS micro-analysis across multiple specimens for reconstructing paleotemperatures. This analytical technique has allowed the reconstruction of reliable Mg/Ca derived paleotemperatures using foraminifera whose bulk trace element ratios demonstrate diagenetic contamination by authigenic coatings. This finding opens the potential for Mg/Ca paleothermometry on other challenging time intervals, and locations, where contaminant coatings have previously inhibited the geochemical analysis of primary foraminiferal calcite. We present new sea surface temperature records from planktic foraminiferal Mg/Ca for the south west Indian Ocean between 13.5 and 9.5 Ma. Absolute estimates of 24–31°C suggest that sea surface temperature was relatively constant through the interval, although our record also suggests two intervals of regional cooling and freshening of surface waters at 11.8 and 10.7 Ma. The late Miocene represented a key interval in the transition of Earth's climate to its modern state, including the development of stronger latitudinal temperature gradients. Our new temperature record suggests that different mechanisms may have been responsible for this cooling. The initial cooling from ~10 Ma at mid to high latitudes in both hemispheres was not associated with significant cooling at low latitudes. On the other hand, the late Miocene cooling between ~7.5 and 5.5 Ma was global in nature and associated with a drawdown in pCO_2 . Further work should therefore explore the mechanisms responsible for the enhanced polar amplification between 10 and 7.5 Ma, and the possibility of carbon cycle feedbacks contributing to the subsequent late Miocene Cooling.

Data Availability Statement

All data from this study can be found in Table 1 and Tables S1–S11, and are deposited in the Zenodo online data repository <https://doi.org/10.5281/zenodo.4472994>.

Acknowledgments

This study uses samples from the Sunbird-1 core provided by BG-Group. We thank Alexandra Nederbragt and Anabel Morte-Rodeñas for laboratory assistance. We thank the reviewers and editor for their insightful comments that improved the manuscript. This research was supported by NERC iCASE studentship BW/22003105 (M.G.N.), and NE/L009633/1 grant to Caroline H. Lear. Open Access funding enabled and organized by Projekt DEAL.

References

- Anand, P., Elderfield, H., & Conte, M. H. (2003). Calibration of Mg/Ca thermometry in planktonic foraminifera from a sediment trap time series. *Paleoceanography*, 18(2). <https://doi.org/10.1029/2002PA000846>
- Aze, T., Ezard, T. H., Purvis, A., Coxall, H. K., Stewart, D. R., Wade, B. S., & Pearson, P. N. (2011). A phylogeny of Cenozoic macroperforate planktonic foraminifera from fossil data. *Biological Reviews*, 86(4), 900–927. <https://doi.org/10.1111/j.1469-185X.2011.00178.x>
- Backman, J., Raffi, I., Rio, D., Fornaciari, E., & Pälike, H. (2012). Biozonation and biochronology of Miocene through Pleistocene calcareous nannofossils from low and middle latitudes. *Newsletters on Stratigraphy*, 45(3), 221–244. <https://doi.org/10.1127/0078-0421/2012/0022>
- Badger, M. P., Lear, C. H., Pancost, R. D., Foster, G. L., Bailey, T. R., Leng, M. J., & Abels, H. A. (2013). CO_2 drawdown following the middle Miocene expansion of the Antarctic Ice Sheet. *Paleoceanography*, 28(1), 42–53. <https://doi.org/10.1002/palo.20015>
- Barker, S., Greaves, M., & Elderfield, H. (2003). A study of cleaning procedures used for foraminiferal Mg/Ca paleothermometry. *Geochemistry, Geophysics, Geosystems*, 4(9). <https://doi.org/10.1029/2003GC000559>

- Bemis, B. E., Spero, H. J., Bijma, J., & Lea, D. W. (1998). Reevaluation of the oxygen isotopic composition of planktonic foraminifera: Experimental results and revised paleotemperature equations. *Paleoceanography*, 13(2), 150–160. <https://doi.org/10.1029/98PA00070>
- Bertlich, J., Nürnberg, D., Hathorne, E. C., De Nooijer, L. J., Mezger, E. M., Kienast, M., et al. (2018). Salinity control on Na incorporation into calcite tests of the planktonic foraminifera *Trilobatus sacculifer*—evidence from culture experiments and surface sediments. *Biogeosciences*, 15(20), 5991–6018. <https://doi.org/10.5194/bg-2018-164>
- Bolton, C. T., Hernández-Sánchez, M. T., Fuertes, M. A., González-Lemos, S., Abrevaya, L., Mendez-Vicente, A., et al. (2016). Decrease in coccolithophore calcification and CO₂ since the middle Miocene. *Nature Communications*, 7(1), 10284. <https://doi.org/10.1038/ncomms10284>
- Boyer, T. P., Antonov, J. I., Baranova, O. K., Coleman, C., Garcia, H. E., Grodsky, A., et al. (2013). *World ocean database 2013*. National Oceanographic Data Center (U.S.), Ocean Climate Laboratory.
- Boyle, E., & Keigwin, L. (1985). Comparison of Atlantic and Pacific paleochemical records for the last 215,000 years: Changes in deep ocean circulation and chemical inventories. *Earth and Planetary Science Letters*, 76(1), 135–150. [https://doi.org/10.0012/821x/85/\\$03.30](https://doi.org/10.0012/821x/85/$03.30)
- Broecker, W. S., Peng, T.-H., & Beng, Z. (1982). *Tracers in the sea: Lamont-Doherty Geological Observatory*. Columbia University.
- Chen, P., Yu, J., & Jin, Z. (2017). An evaluation of benthic foraminiferal U/Ca and U/Mn proxies for deep ocean carbonate chemistry and redox conditions. *Geochemistry, Geophysics, Geosystems*, 18(2), 617–630. <http://doi.org/10.1002/2016GC006730>
- Coggon, R. M., Teagle, D. A., Smith-Duque, C. E., Alt, J. C., & Cooper, M. J. (2010). Reconstructing past seawater Mg/Ca and Sr/Ca from mid-ocean ridge flank calcium carbonate veins. *Science*, 327(5969), 1114–1117. <http://doi.org/10.1126/science.1182252>
- Cramer, B., Miller, K., Barrett, P., & Wright, J. (2011). Late Cretaceous–Neogene trends in deep ocean temperature and continental ice volume: reconciling records of benthic foraminiferal geochemistry ($\delta^{18}\text{O}$ and Mg/Ca) with sea level history. *Journal of Geophysical Research*, 116(C12). <https://doi.org/10.1029/2011JC007255>
- Cramwinckel, M. J., Huber, M., Kocken, I. J., Agnini, C., Bijl, P. K., Bohaty, S. M., et al. (2018). Synchronous tropical and polar temperature evolution in the Eocene. *Nature*, 559(7714), 382–386. <http://doi.org/10.1038/s41586-018-0272-2>
- Creech, J. B., Baker, J. A., Hollis, C. J., Morgans, H. E. G., & Smith, E. G. C. (2010). Eocene sea temperatures for the mid-latitude southwest Pacific from Mg/Ca ratios in planktonic and benthic foraminifera. *Earth and Planetary Science Letters*, 299(3–4), 483–495. <https://doi.org/10.1016/j.epsl.2010.09.039>
- de Nooijer, L. J., Hathorne, E. C., Reichart, G.-J., Langer, G., & Bijma, J. (2014). Variability in calcitic Mg/Ca and Sr/Ca ratios in clones of the benthic foraminifer *Ammonia tepida*. *Marine Micropaleontology*, 107, 32–43. <https://doi.org/10.1016/j.marmicro.2014.02.002>
- de Nooijer, L. J., van Dijk, I., Toyofuku, T., & Reichart, G. J. (2017). The Impacts of Seawater Mg/Ca and Temperature on Element Incorporation in Benthic Foraminiferal Calcite. *Geochemistry, Geophysics, Geosystems*, 18(10), 3617–3630. <http://doi.org/10.1002/2017GC007183>
- Delaney, M. L., Be, A. W. H., & Boyle, E. A. (1985). Li, Sr, Mg, and Na in foraminiferal calcite shells from laboratory culture sediment traps, and sediment cores. *Geochimica et Cosmochimica Acta*, 49(6), 1327–1341. [https://doi.org/10.1016/0016-7037\(85\)90284-4](https://doi.org/10.1016/0016-7037(85)90284-4)
- Detlef, H., Sosdian, S. M., Kender, S., Lear, C. H., & Hall, I. R. (2019). Multi-elemental composition of authigenic carbonates in benthic foraminifera from the eastern Bering Sea continental margin (International Ocean Discovery Program Site U1343). *Geochimica et Cosmochimica Acta*, 268, 1–21. <https://doi.org/10.1016/j.gca.2019.09.025>
- Dickson, J. A. D. (2002). Fossil Echinoderms as monitor of the Mg/Ca Ratio of Phanerozoic Oceans. *Science*, 298(5596), 1222–1224. <http://doi.org/10.1126/science.1075882>
- Eggins, S., De Deckker, P., & Marshall, J. (2003). Mg/Ca variation in planktonic foraminifera tests: implications for reconstructing paleo-seawater temperature and habitat migration. *Earth and Planetary Science Letters*, 212(3), 291–306. [https://doi.org/10.1016/S0012-821X\(03\)00283-8](https://doi.org/10.1016/S0012-821X(03)00283-8)
- Eggins, S. M., Sadekov, A., & De Deckker, P. (2004). Modulation and daily banding of Mg/Ca in *Orbulina universa* tests by symbiont photosynthesis and respiration: A complication for seawater thermometry? *Earth and Planetary Science Letters*, 225(3), 411–419. <https://doi.org/10.1016/j.epsl.2004.06.019>
- Evans, D., Bhatia, R., Stoll, H., & Müller, W. (2015). LA-ICPMS Ba/Ca analyses of planktic foraminifera from the Bay of Bengal: Implications for late Pleistocene orbital control on monsoon freshwater flux. *Geochemistry, Geophysics, Geosystems*, 16(8), 2598–2618. <https://doi.org/10.1002/2015GC005822>
- Evans, D., Brierley, C., Raymo, M. E., Erez, J., & Müller, W. (2016). Planktic foraminifera shell chemistry response to seawater chemistry: Pliocene-Pleistocene seawater Mg/Ca, temperature and sea level change. *Earth and Planetary Science Letters*, 438, 139–148. <http://doi.org/10.1016/j.epsl.2016.01.013>
- Evans, D., Erez, J., Oron, S., & Müller, W. (2015). Mg/Ca-temperature and seawater-test chemistry relationships in the shallow-dwelling large benthic foraminifera *Operculina ammonoides*. *Geochimica et Cosmochimica Acta*, 148, 325–342. <https://doi.org/10.1016/j.gca.2014.09.039>
- Evans, D., & Müller, W. (2012). Deep time foraminifera Mg/Ca paleothermometry: Nonlinear correction for secular change in seawater Mg/Ca. *Paleoceanography*, 27(4). <https://doi.org/10.1029/2012PA002315>
- Evans, D., & Müller, W. (2018). Automated extraction of a five-year LA-ICP-MS trace element dataset of ten common glass and carbonate reference materials: Long-term data quality, optimisation and laser cell homogeneity. *Geostandards and Geoanalytical Research*, 42, 159–188. <https://doi.org/10.1111/ggr.12204>
- Evans, D., Sagoo, N., Renema, W., Cotton, L. J., Müller, W., Todd, J. A., et al. (2018). Eocene greenhouse climate revealed by coupled clumped isotope-Mg/Ca thermometry. *Proceedings of the National Academy of Sciences of the United States of America*, 115(6), 1174–1179. <http://doi.org/10.1073/pnas.1714744115>
- Evans, D., Wade, B. S., Henahan, M., Erez, J., & Müller, W. (2016). Revisiting carbonate chemistry controls on planktic foraminifera Mg/Ca: Implications for sea surface temperature and hydrology shifts over the Paleocene-Eocene thermal maximum and Eocene-Oligocene transition. *Climate of the Past*, 12(4), 819–835. <http://doi.org/10.5194/cp-12-819-2016>
- Farrell, J. W., Raffi, I., Janecek, T. R., Murray, D. W., Levitan, M., Dadey, K. A., et al. (1995). Late Neogene sedimentation patterns in the eastern equatorial Pacific Ocean. In N. G. Pisias, L. A. Mayer, T. R. Janacek, A. Palmer-Julson, & T. H. van Andel (Eds.), *Proceedings of the Ocean Drilling Program, Scientific Results* (Vol. 138). Ocean Drilling Program. https://www.researchgate.net/profile/Mitchell_Lyle/publication/284193939_Late_Neogene_Sedimentation_Patterns_in_the_Eastern_Equatorial_Pacific_Ocean/links/56fd2d3808aea3275abb9ca2/Late-Neogene-Sedimentation-Patterns-in-the-Eastern-Equatorial-Pacific-Ocean.pdf
- Fehrenbacher, J. S., & Martin, P. A. (2014). Exploring the dissolution effect on the intrashell Mg/Ca variability of the planktic foraminifer *Globigerinoides ruber*. *Paleoceanography*, 29(9), 854–868. <https://doi.org/10.1002/2013PA002571>
- Fehrenbacher, J. S., Spero, H. J., Russell, A. D., Vetter, L., & Eggins, S. (2015). Optimizing LA-ICP-MS analytical procedures for elemental depth profiling of foraminifera shells. *Chemical Geology*, 407–408, 2–9. <http://doi.org/10.1016/j.chemgeo.2015.04.007>

- Foster, G. L., Lear, C. H., & Rae, J. W. B. (2012). The evolution of pCO₂, ice volume and climate during the middle Miocene. *Earth and Planetary Science Letters*, 341–344, 243–254. <https://doi.org/10.1016/j.epsl.2012.06.007>
- Foster, G. L., & Rae, J. W. (2015). Reconstructing Ocean pH with Boron Isotopes in Foraminifera. *Annual Review of Earth and Planetary Sciences*, 44, 207–237. https://www.annualreviews.org/doi/full/10.1146/annurev-earth-060115-012226#_i63
- Geerken, E., De Nooijer, L. J., Van Dijk, I., & Reichert, G.-J. (2018). Impact of salinity on element incorporation in two benthic foraminiferal species with contrasting magnesium contents. *Biogeosciences*, 15(7), 2205–2218. <https://doi.org/10.5194/bg-15-2205-2018>
- Gray, W. R., & Evans, D. (2019). Nonthermal influences on Mg/Ca in planktonic foraminifera: a review of culture studies and application to the Last Glacial Maximum. *Paleoceanography and Paleoclimatology*, 34(3), 306–315. <https://doi.org/10.1029/2018PA003517>
- Gray, W. R., Weldeab, S., Lea, D. W., Rosenthal, Y., Gruber, N., Donner, B., & Fischer, G. (2018). The effects of temperature, salinity, and the carbonate system on Mg/Ca in Globigerinoides ruber (white): A global sediment trap calibration. *Earth and Planetary Science Letters*, 482, 607–620. <http://doi.org/10.1016/j.epsl.2017.11.026>
- Greenop, R., Foster, G. L., Wilson, P. A., & Lear, C. H. (2014). Middle Miocene climate instability associated with high-amplitude CO₂ variability. *Paleoceanography*, 29(9), 845–853. <https://doi.org/10.1002/2014PA002653>
- Greenop, R., Hain, M. P., Sosdian, S. M., Oliver, K. I. C., Goodwin, P., Chalk, T. B., et al. (2017). A record of Neogene seawater δ¹¹B reconstructed from paired δ¹¹B analyses on benthic and planktic foraminifera. *Climate of the Past*, 13(2), 149–170. <https://doi.org/10.5194/cp-13-149-2017>
- Guillong, M., Meier, L. D., Allan, M., Heinrich, A. C., & Yardley, B. (2008). SILLS: A MATLAB-based program for the reduction of laser ablation ICP-MS data of homogeneous materials and inclusions. *Mineralogical Association of Canada Short Course*, 40, 328–333. https://ethz.ch/content/dam/ethz/special-interest/erdw/geopetro/mineralsystems-dam/documents/MAC_SC_40_Sills_description.pdf
- Hasenfratz, A. P., Martínez-García, A., Jaccard, S. L., Vance, D., Wälle, M., Greaves, M., & Haug, G. H. (2016). Determination of the Mg/Mn ratio in foraminiferal coatings: An approach to correct Mg/Ca temperatures for Mn-rich contaminant phases. *Earth and Planetary Science Letters*, 457, 335–347. <https://doi.org/10.1016/j.epsl.2016.10.004>
- Hasiuk, F. J., & Lohmann, K. C. (2010). Application of calcite Mg partitioning functions to the reconstruction of paleocean Mg/Ca. *Geochimica et Cosmochimica Acta*, 74(23), 6751–6763. <https://doi.org/10.1016/j.gca.2010.07.030>
- Henehan, M. J., Rae, J. W. B., Foster, G. L., Erez, J., Prentice, K. C., Kucera, M., et al. (2013). Calibration of the boron isotope proxy in the planktonic foraminifera Globigerinoides ruber for use in palaeo-CO₂ reconstruction. *Earth and Planetary Science Letters*, 364, 111–122. <https://doi.org/10.1016/j.epsl.2012.12.029>
- Herbert, T. D., Lawrence, K. T., Tzanova, A., Peterson, L. C., Caballero-Gill, R., & Kelly, C. S. (2016). Late Miocene global cooling and the rise of modern ecosystems. *Nature Geoscience*, 9, 843–847. <https://doi.org/10.1038/ngeo2813>
- Hines, B. R., Hollis, C. J., Atkins, C. B., Baker, J. A., Morgans, H. E. G., & Strong, P. C. (2017). Reduction of oceanic temperature gradients in the early Eocene Southwest Pacific Ocean. *Palaeogeography, Palaeoclimatology, Palaeoecology*, 475, 41–54. <https://doi.org/10.1016/j.palaeo.2017.02.037>
- Holland, K., Branson, O., Haynes, L. L., Hönisch, B., Allen, K. A., Russell, A. D., et al. (2020). Constraining multiple controls on planktic foraminifera Mg/Ca. *Geochimica et Cosmochimica Acta*, 273, 116–136. <https://doi.org/10.1016/j.gca.2020.01.015>
- Hollis, C., Dunkley Jones, T., Anagnostou, E., Bijl, P., Cramwinckel, M., Cui, Y., et al. (2019). The DeepMIP contribution to PMIP4: methodologies for selection, compilation and analysis of latest Paleocene and early Eocene climate proxy data, incorporating version 0.1 of the DeepMIP database. *Geoscientific Model Development Discussions*, 2019, 1–98. <https://doi.org/10.5194/gmd-12-3149-2019>
- Hollis, C., Hines, B., Littler, K., Villasante-Marcos, V., Kulhanek, D., Strong, C., et al. (2015). The Paleocene–Eocene thermal maximum at DSDP site 277, Campbell Plateau, southern Pacific Ocean. *Climate of the Past*, 11(7), 1009–1025. <https://doi.org/10.5194/cp-11-1009-2015>
- Hönisch, B., Allen, K. A., Lea, D. W., Spero, H. J., Eggins, S. M., Arbuszewski, J., et al. (2013). The influence of salinity on Mg/Ca in planktic foraminifera—Evidence from cultures, core-top sediments and complementary δ¹⁸O. *Geochimica et Cosmochimica Acta*, 121, 196–213. <https://doi.org/10.1016/j.gca.2013.07.028>
- Horita, J., Zimmermann, H., & Holland, H. D. (2002). Chemical evolution of seawater during the Phanerozoic: Implications from the record of marine evaporites. *Geochimica et Cosmochimica Acta*, 66(21), 3733–3756. [https://doi.org/10.1016/S0016-7037\(01\)00884-5](https://doi.org/10.1016/S0016-7037(01)00884-5)
- Huang, Y., Clemens, S. C., Liu, W., Wang, Y., & Prell, W. L. (2007). Large-scale hydrological change drove the late Miocene C4 plant expansion in the Himalayan foreland and Arabian Peninsula. *Geology*, 35(6), 531–534. <https://doi.org/10.1130/G23666A.1>
- Jiang, S., Wise, S., & Wang, Y. (2007). Cause of the middle/late Miocene carbonate crash: Dissolution or low productivity. Paper presented at the Proceedings of the Ocean Drilling Program, Scientific Results, (Vol. 206, pp. 1–24). College Station, Texas: Ocean Drilling Program. http://www-odp.tamu.edu/publications/206_sr/013/013.htm
- Jochum, K. P., Weis, U., Stoll, B., Kuzmin, D., Yang, Q., Raczek, I., et al. (2011). Determination of reference values for NIST SRM 610–617 glasses following ISO guidelines. *Geostandards and Geoanalytical Research*, 35(4), 397–429. <https://doi.org/10.1111/j.1751-908X.2011.00120.x>
- Jochum, K. P., Wilson, S. A., Abouchami, W., Amini, M., Chmeleff, J., Eisenhauer, A., et al. (2011). GSD-1G and MPI-DING reference glasses for in situ and bulk isotopic determination. *Geostandards and Geoanalytical Research*, 35(2), 193–226. <https://doi.org/10.1111/j.1751-908X.2010.00114.x>
- Keller, G. (1985). Depth stratification of planktonic foraminifera in the Miocene ocean. *The Miocene Ocean: Paleoceanography and Biogeography*, 163, 177–196.
- Keller, G., & Barron, J. A. (1987). Paleodepth distribution of Neocene deep-sea hiatuses. *Paleoceanography*, 2(6), 697–713. <https://doi.org/10.1029/PA002i006p00697>
- Knorr, G., Butzin, M., Micheels, A., & Lohmann, G. (2011). A warm Miocene climate at low atmospheric CO₂ levels. *Geophysical Research Letters*, 38(20). <https://doi.org/10.1029/2011GL048873>
- Koho, K., de Nooijer, L., & Reichert, G. (2015). Combining benthic foraminiferal ecology and shell Mn/Ca to deconvolve past bottom water oxygenation and paleoproductivity. *Geochimica et Cosmochimica Acta*, 165, 294–306. <https://doi.org/10.1016/j.gca.2015.06.003>
- Kisakürek, B., Eisenhauer, A., Böhm, F., Garbe-Schönberg, D., & Erez, J. (2008). Controls on shell Mg/Ca and Sr/Ca in cultured planktonic foraminifera, Globigerinoides ruber (white). *Earth and Planetary Science Letters*, 273(3–4), 260–269. <https://doi.org/10.1016/j.epsl.2008.06.026>
- LaRiviere, J. P., Ravelo, A. C., Crimmins, A., Dekens, P. S., Ford, H. L., Lyle, M., & Wara, M. W. (2012). Late Miocene decoupling of oceanic warmth and atmospheric carbon dioxide forcing. *Nature*, 486(7401), 97. <https://doi.org/10.1038/nature11200>
- Lear, C. H., Coxall, H. K., Foster, G. L., Lunt, D. J., Mawbey, E. M., Rosenthal, Y., et al. (2015). Neogene ice volume and ocean temperatures: Insights from infaunal foraminiferal Mg/Ca paleothermometry. *Paleoceanography*, 30(11), 1437–1454. <https://doi.org/10.1002/2015PA002833>
- Lear, C. H., Mawbey, E. M., & Rosenthal, Y. (2010). Cenozoic benthic foraminiferal Mg/Ca and Li/Ca records: Toward unlocking temperatures and saturation states. *Paleoceanography*, 25(4). <https://doi.org/10.1029/2009pa001880>

- Lear, C. H., Rosenthal, Y., & Slowey, N. (2002). Benthic foraminiferal Mg/Ca-paleothermometry: A revised core-top calibration. *Geochimica et Cosmochimica Acta*, 66(19), 3375–3387. [https://doi.org/10.1016/S0016-7037\(02\)00941-9](https://doi.org/10.1016/S0016-7037(02)00941-9)
- LeGrande, A. N., & Schmidt, G. A. (2006). Global gridded data set of the oxygen isotopic composition in seawater. *Geophysical Research Letters*, 33(12). <https://doi.org/10.1029/2006GL026011>
- Longerich, H. P., Jackson, S. E., & Günther, D. (1996). Inter-laboratory note. Laser ablation inductively coupled plasma mass spectrometric transient signal data acquisition and analyte concentration calculation. *Journal of Analytical Atomic Spectrometry*, 11(9), 899–904. <https://doi.org/10.1039/JA9961100899>
- Lübbbers, J., Kuhnt, W., Holbourn, A. E., Bolton, C. T., Gray, E., Usui, Y., et al. (2019). The middle to late Miocene “Carbonate Crash” in the equatorial Indian Ocean. *Paleoceanography and Paleoclimatology*, 34(5), 813–832. <https://doi.org/10.1029/2018PA003482>
- Lunt, D. J., Flecker, R., Valdes, P. J., Salzmann, U., Gladstone, R., & Haywood, A. M. (2008). A methodology for targeting palaeo proxy data acquisition: A case study for the terrestrial late Miocene. *Earth and Planetary Science Letters*, 271(1), 53–62. <https://doi.org/10.1016/j.epsl.2008.03.035>
- Lyle, M., Dadey, K. A., & Farrell, J. W. (1995). The Late Miocene (11–8 Ma) Eastern Pacific Carbonate Crash: Evidence for reorganization of deep-water Circulation by the closure of the Panama Gateway. Proceedings of the Ocean Drilling Program, Scientific Results, (Vol. 138). College Station, Texas: Ocean Drilling Project. <http://citeseerx.ist.psu.edu/viewdoc/download?doi=10.1.1.558.1733&rep=rep1&type=pdf>
- Mayk, D., Fietzke, J., Anagnostou, E., & Paytan, A. (2020). LA-MC-ICP-MS study of boron isotopes in individual planktonic foraminifera: A novel approach to obtain seasonal variability patterns. *Chemical Geology*, 531, 119351. <https://doi.org/10.1016/j.chemgeo.2019.119351>
- Müller, P. J., Kirst, G., Ruhland, G., Von Storch, I., & Rosell-Melé, A. (1998). Calibration of the alkenone paleotemperature index U₃₇ K' based on core-tops from the eastern South Atlantic and the global ocean (60 N–60 S). *Geochimica et Cosmochimica Acta*, 62(10), 1757–1772. [https://doi.org/10.1016/S0016-7037\(98\)00097-0](https://doi.org/10.1016/S0016-7037(98)00097-0)
- Nairn, M. (2018). *Mid-Late Miocene climate constrained by a new Laser Ablation ICP-MS set up*. (PhD thesis.). Cardiff University.
- Nürnberg, D., Bijma, J., & Hemleben, C. (1996). Assessing the reliability of magnesium in foraminiferal calcite as a proxy for water mass temperatures. *Geochimica et Cosmochimica Acta*, 60(5), 803–814.
- Pagani, M., Freeman, K. H., & Arthur, M. A. (1999). Late Miocene atmospheric CO₂ concentrations and the expansion of C₄ grasses. *Science*, 285(5429), 876–879. <https://doi.org/10.1126/science.285.5429.876>
- Pälike, H., Lyle, M. W., Nishi, H., Raffi, I., Ridgwell, A., Gamage, K., et al. (2012). A Cenozoic record of the equatorial Pacific carbonate compensation depth. *Nature*, 488(7413), 609–614. <https://doi.org/10.1038/nature11360>
- Pearson, P. N., & Burgess, C. E. (2008). Foraminifer test preservation and diagenesis: comparison of high latitude Eocene sites. *Geological Society, London, Special Publications*, 303(1), 59–72. <https://doi.org/10.1144/SP303.5>
- Pearson, P. N., Ditchfield, P. W., Singano, J., Harcourt-Brown, K. G., Nicholas, C. J., Olsson, R. K., et al. (2001). Warm tropical sea surface temperatures in the Late Cretaceous and Eocene epochs. *Nature*, 413(6855), 481–487. <https://doi.org/10.1038/35097000>
- Pena, L., Calvo, E., Cacho, I., Eggins, S., & Pelejero, C. (2005). Identification and removal of Mn-Mg-rich contaminant phases on foraminiferal tests: Implications for Mg/Ca past temperature reconstructions. *Geochemistry, Geophysics, Geosystems*, 6(9). <https://doi.org/10.1029/2005GC000930>
- Petersen, J., Barras, C., Bézou, A., La, C., De Noijer, L. J., Meysman, F. J. R., et al. (2018). Mn/Ca intra- and inter-test variability in the benthic foraminifer *Ammonia tepida*. *Biogeosciences*, 15(1), 331–348. <https://doi.org/10.5194/bg-15-331-2018>
- Pisias, N., & Mix, A. (1988). Aliasing of the geologic record and the search for long-period Milankovitch cycles (3).
- Pound, M. J., Haywood, A. M., Salzmann, U., Riding, J. B., Lunt, D. J., & Hunter, S. J. (2011). A Tortonian (Late Miocene, 11.61–7.25Ma) global vegetation reconstruction. *Palaeogeography, Palaeoclimatology, Palaeoecology*, 300(1), 29–45. <https://doi.org/10.1016/j.palaeo.2010.11.029>
- Raffi, I., Wade, B. S., Pälike, H., Beu, A. G., Cooper, R., Crundwell, M. P., et al. (2020). The Neogene period. In F. M. Gradstein, J. G. Ogg, M. D. Schmitz, & G. M. Ogg (Eds.), *Geologic time scale 2020* (pp. 1141–1215). Elsevier. <https://doi.org/10.1016/B978-0-12-824360-2.00029-2>
- Raitzsch, M., Kuhnert, H., Hathorne, E. C., Groeneveld, J., & Bickert, T. (2011). U/Ca in benthic foraminifera: A proxy for the deep-sea carbonate saturation. *Geochemistry, Geophysics, Geosystems*, 12(6). <https://doi.org/10.1029/2010GC003344>
- Rathmann, S., Hess, S., Kuhnert, H., & Mulitza, S. (2004). Mg/Ca ratios of the benthic foraminifera *Oridorsalis umbonatus* obtained by laser ablation from core top sediments: Relationship to bottom water temperature. *Geochemistry, Geophysics, Geosystems*, 5(12). <https://doi.org/10.1029/2004gc000808>
- Reichart, G.-J., Jorissen, F., Anschutz, P., & Mason, P. R. (2003). Single foraminiferal test chemistry records the marine environment. *Geology*, 31(4), 355–358. [https://doi.org/10.1130/0091-7613\(2003\)031<0355:SFTCRT>2.0.CO;2](https://doi.org/10.1130/0091-7613(2003)031<0355:SFTCRT>2.0.CO;2)
- Rosenthal, Y., Boyle, E. A., & Slowey, N. (1997). Temperature control on the incorporation of magnesium, strontium, fluorine, and cadmium into benthic foraminiferal shells from Little Bahama Bank: Prospects for thermocline paleoceanography. *Geochimica et Cosmochimica Acta*, 61(17), 3633–3643.
- Rousselle, G., Beltran, C., Sicre, M.-A., Raffi, I., & De Rafélis, M. (2013). Changes in sea-surface conditions in the Equatorial Pacific during the middle Miocene–Pliocene as inferred from coccolith geochemistry. *Earth and Planetary Science Letters*, 361, 412–421. <https://doi.org/10.1016/j.epsl.2012.11.003>
- Russell, A. D., Hönisch, B., Spero, H. J., & Lea, D. W. (2004). Effects of seawater carbonate ion concentration and temperature on shell U, Mg, and Sr in cultured planktonic foraminifera. *Geochimica et Cosmochimica Acta*, 68(21), 4347–4361. <https://doi.org/10.1016/j.gca.2004.03.013>
- Sadekov, A., Eggins, S. M., De Deckker, P., & Kroon, D. (2008). Uncertainties in seawater thermometry deriving from intratest and intertest Mg/Ca variability in *Globigerinoides ruber*. *Paleoceanography*, 23(1). <https://doi.org/10.1029/2007pa001452>
- Sadekov, A. Y., Eggins, S. M., & De Deckker, P. (2005). Characterization of Mg/Ca distributions in planktonic foraminifera species by electron microprobe mapping. *Geochemistry, Geophysics, Geosystems*, 6(12). <https://doi.org/10.1029/2005GC000973>
- Schiebel, R., & Hemleben, C. (2017). *Planktic foraminifera in the modern ocean*. Berlin: Springer.
- Schlitzer, R. (2020). *Ocean Data View*. <https://odv.awi.de/>
- Seki, O., Schmidt, D. N., Schouten, S., Hopmans, E. C., Sinninghe Damsté, J. S., & Pancost, R. D. (2012). Paleoceanographic changes in the Eastern Equatorial Pacific over the last 10 Myr. *Paleoceanography*, 27(3), n/a–n/a. <https://doi.org/10.1029/2011pa002158>
- Sexton, P. F., Wilson, P. A., & Pearson, P. N. (2006). Microstructural and geochemical perspectives on planktic foraminiferal preservation: “Glassy” versus “Frosty”. *Geochemistry, Geophysics, Geosystems*, 7(12). <https://doi.org/10.1029/2006GC001291>
- Sosdian, S. M., Greenop, R., Hain, M. P., Foster, G. L., Pearson, P. N., & Lear, C. H. (2018). Constraining the evolution of Neogene ocean carbonate chemistry using the boron isotope pH proxy. *Earth and Planetary Science Letters*, 498, 362–376. <https://doi.org/10.1016/j.epsl.2018.06.017>

- Sosdian, S. M., & Lear, C. H. (2020). Initiation of the Western Pacific Warm Pool at the Middle Miocene climate transition? *Paleoceanography and Paleoclimatology*, 35(12), e2020PA003920. <https://doi.org/10.1029/2020PA003920>
- Stewart, D. R. M., Pearson, P. N., Ditchfield, P. W., & Singano, J. M. (2004). Miocene tropical Indian Ocean temperatures: evidence from three exceptionally preserved foraminiferal assemblages from Tanzania. *Journal of African Earth Sciences*, 40(3), 173–189. <https://doi.org/10.1016/j.jafrearsci.2004.09.001>
- Stoll, H. M., Guitian, J., Hernandez-Almeida, I., Mejia, L. M., Phelps, S., Polissar, P., et al. (2019). Upregulation of phytoplankton carbon concentrating mechanisms during low CO₂ glacial periods and implications for the phytoplankton pCO₂ proxy. *Quaternary Science Reviews*, 208, 1–20. <https://doi.org/10.1016/j.quascirev.2019.01.012>
- Super, J. R., Thomas, E., Pagani, M., Huber, M., O'Brien, C., & Hull, P. M. (2018). North Atlantic temperature and p CO₂ coupling in the early-middle Miocene. *Geology*, 46(6), 519–522. <https://doi.org/10.1130/G40228.1>
- Thil, F., Blamart, D., Assailly, C., Lazareth, C. E., Leblanc, T., Butsher, J., & Douville, E. (2016). Development of laser ablation multi-collector inductively coupled plasma mass spectrometry for boron isotopic measurement in marine biocarbonates: New improvements and application to a modern *Porites* coral. *Rapid Communications in Mass Spectrometry*, 30(3), 359–371. <https://doi.org/10.1002/rcm.7448>
- van Hinsbergen, D. J., de Groot, L. V., van Schaik, S. J., Spakman, W., Bijl, P. K., Sluijs, A., et al. (2015). A paleolatitude calculator for paleoclimate studies. *PloS One*, 10(6), e0126946. <https://doi.org/10.1371/journal.pone.0126946>
- Vetter, L., Kozdon, R., Mora, C. I., Eggins, S. M., Valley, J. W., Hönisch, B., & Spero, H. J. (2013). Micron-scale intrashell oxygen isotope variation in cultured planktic foraminifers. *Geochimica et Cosmochimica Acta*, 107, 267–278. <https://doi.org/10.1016/j.gca.2012.12.046>
- von der Heydt, A., & Dijkstra, H. A. (2006). Effect of ocean gateways on the global ocean circulation in the late Oligocene and early Miocene. *Paleoceanography*, 21(1). <https://doi.org/10.1029/2005pa001149>
- Wade, B. S., Pearson, P. N., Berggren, W. A., & Pälike, H. (2011). Review and revision of Cenozoic tropical planktonic foraminiferal biostratigraphy and calibration to the geomagnetic polarity and astronomical time scale. *Earth-Science Reviews*, 104(1), 111–142. <https://doi.org/10.1016/j.earscirev.2010.09.003>
- Westerhold, T., Marwan, N., Drury, A. J., Liebrand, D., Agnini, C., Anagnostou, E., et al. (2020). An astronomically dated record of Earth's climate and its predictability over the last 66 million years. *Science*, 369(6509), 1383–1387. <https://doi.org/10.1126/science.aba6853>
- Yu, J., & Elderfield, H. (2008). Mg/Ca in the benthic foraminifera *Cibicides wuellerstorfi* and *Cibicides mundulus*: Temperature versus carbonate ion saturation. *Earth and Planetary Science Letters*, 276(1), 129–139. <https://doi.org/10.1016/j.epsl.2008.09.015>
- Zachos, J. C., Stott, L. D., & Lohmann, K. C. (1994). Evolution of early Cenozoic marine temperatures. *Paleoceanography*, 9(2), 353–387. <https://doi.org/10.1029/93PA03266>
- Zhang, Y. G., Pagani, M., Liu, Z., Bohaty, S. M., & DeConto, R. (2013). A 40-million-year history of atmospheric CO₂. *Philosophical Transactions of the Royal Society A: Mathematical, Physical and Engineering Sciences*, 371(2001), 20130096. <https://doi.org/10.1098/rsta.2013.0096>
- Zhang, Y. G., Pagani, M., & Liu, Z. (2014). A 12-million-year temperature history of the tropical Pacific Ocean. *Science*, 344(6179), 84–87. <https://doi.org/10.1126/science.1246172>

References From the Supporting Information

- Lemarchand, D., Gaillardet, J., Lewin, E., & Allegre, C. (2002). Boron isotope systematics in large rivers: implications for the marine boron budget and paleo-pH reconstruction over the Cenozoic. *Chemical Geology*, 190(1), 123–140. [https://doi.org/10.1016/S0009-2541\(02\)00114-6](https://doi.org/10.1016/S0009-2541(02)00114-6)
- Raitzsch, M., & Hönisch, B. (2013). Cenozoic boron isotope variations in benthic foraminifers. *Geology*, 41(5), 591–594. <https://doi.org/10.1130/g34031.1>